Thesis for The Degree of Licentiate of Engineering

Fluctuations and nonequilibrium thermodynamics in electronic nanosystems

Ludovico Tesser

Department of Microtechnology and Nanoscience (MC2)
Applied Quantum Physics Laboratory
Chalmers University of Technology
Gothenburg, Sweden, 2022

Fluctuations and nonequilibrium thermodynamics in electronic nanosystems

Ludovico Tesser

Thesis for the degree of Licentiate of Engineering
ISSN 1652-0769
Technical Report No MC2-456

Applied Quantum Physics Laboratory
Department of Microtechnology and Nanoscience (MC2)
Chalmers University of Technology
SE-412 96 Göteborg, Sweden
Phone: +46(0)31 772 1000

Cover: The author's attempt to artistically illustrate transport in an out-of-equilibrium two terminal system.

Printed by Chalmers Digitaltryck,
Gothenburg, Sweden 2022.

Fluctuations and nonequilibrium thermodynamics in electronic nanosystems

Ludovico Tesser

Applied Quantum Physics Laboratory
Department of Microtechnology and Nanoscience (MC2)
Chalmers University of Technology

Abstract

In the last decades thermodynamics has seen a resurgence because of the interesting phenomena that happen in small-scale systems. Indeed, in nanoscale devices, quantum effects and fluctuations cannot generally be neglected and influence both the transport and their thermodynamic performance. In particular, most devices operate *out of equilibrium*, where additional fluctuations emerge and nonthermal distributions may occur. Using the scattering theory formalism, the articles discussed in this thesis contribute to two different aspects of transport in out-of-equilibrium mesoscopic conductors, namely current fluctuations under out-of-equilibrium conditions and the effect of nonequilibrium (or nonthermal) distributions as a resource for thermodynamic operations.

On the one hand, we study the out-of-equilibrium fluctuations in the absence of current, focusing on the shot noise for heat, spin, and charge currents. In particular, we prove the existence of a general bound, namely that, when the zero average charge current is achieved using a temperature and a voltage bias, the charge shot noise is *always* smaller than the thermal noise.

On the other hand, we introduce a novel quantum transport model to analyze the performance of a hot-carrier solar cell. This device combines aspects of thermoelectric and photovoltaic devices to enhance its performance. Using our model, we show that exploiting the nonequilibrium resource of a nonthermal distribution improves power production.

Keywords: Fluctuations and noise; Charge, heat and spin transport; Shot noise; Nonequilibrium thermodynamics; Mesoscopic thermoelectricity; Hot-carrier solar cell

List of Publications

Appended publications

This thesis is based on the following publications:

[I] J. Eriksson, M. Acciai, **L. Tesser**, J. Splettstoesser, *General Bounds on Electronic Shot Noise in the Absence of Currents*
Phys. Rev. Lett. 127, 136801 (2021).

[II] **L. Tesser**, M. Acciai, C. Spånslätt, J. Monsel, J. Splettstoesser, *Charge, spin, and heat shot noises in the absence of average currents: Conditions on bounds at zero and finite frequencies*
Draft, soon to be submitted.

[III] **L. Tesser**, R. S. Whitney, J. Splettstoesser, *Thermodynamic performance of hot-carrier solar cells: A quantum transport model*
arXiv:2209.09524 (2022).

In the remainder of the thesis, we will refer to the listed papers according to their numerals as [I], [II], and [III] respectively.

Other publications

The following publications was published during my PhD studies. However, it is not appended to this thesis, due to different formalism.

[a] **L. Tesser**, B. Bhandari, P. A. Erdman, E. Paladino, R. Fazio, F. Taddei, *Heat rectification through single and coupled quantum dots*
New J. Phys. 24, 035001 (2022).

Acknowledgments

First and foremost, I want to thank my supervisor Janine Splettstößer, who gave me the opportunity to study as a PhD candidate in her group. Thank you for your continuous and unwavering support and for your contagious enthusiasm in doing science.

A special thank goes to Matteo Acciai, with whom I had fruitful and insightful discussions and who had plenty of patience while I was looking for inequalities.

I would also like to thank Robert Whitney, Christian Spånslätt, and Juliette Monsel for the useful discussions and for the helpful contributions to my project.

Finally, I want to acknowledge all who bore discussing science with me. I am sure I learned something from each and every of you.

Contents

Chapter 1

Introduction

This thesis and the appended papers deal with electronic *mesoscopic* systems *out of equilibrium*. Mesoscopic systems are attracting increasing interest as devices, for example transistors, become smaller and quantum effects affect their behavior [1]. In particular, while quantum mechanics worsen the performance of classical devices, it offers new possibilities for novel and advantageous technologies both from a theoretical and an experimental point of view, for example quantum computing [2]. This is made possible by the low temperatures reached in such quantum devices [3], ranging from 100 K to sub-Kelvin temperatures, which allow quantum coherence to take place. The mesoscopic devices considered in this thesis are such that their dimension is smaller than the electron coherence and thermalization lengths. This makes the electron wavefunction propagate through the device without losing coherence, thereby allowing quantum mechanical effects to take place in the device. Such kind of propagation is studied in the wider field of *quantum transport*, whose research is focused on currents flowing under quantum effects. The currents investigated are often charge and heat currents, which are fundamental for characterizing the thermodynamic properties of electronic systems, and are crucial for thermoelectricity [4]. Nonetheless, additional kinds of currents are investigated depending on the system. For instance, spin currents are fundamental in the field of spintronics [5].

However, for transport to happen and currents to be non-zero, the system needs to be out of equilibrium. In fact, equilibrium systems can be quite uninteresting for their lack of dynamics and resources. This is illustrated by the second law of thermodynamics, which does not allow entropy decrease, when applied to the equilibrium state, which has maximum entropy. Therefore, out-of-equilibrium systems are necessary for many useful tasks, for example refrigeration and power production. Mesoscopic devices improve the performance of such tasks by exploiting quantum effects and offer the possibility of local operation, for example on-chip cooling [6], thanks to their small size. Concretely, most devices operate out of equilibrium through the presence of some bias, for example voltage or temperature biases, driving the currents. This is the case in quantum heat engines [7, 8], refrigerators [9, 10], current rectifiers [11–13], and

many more [14–17]. However, it is also possible to induce currents by using the nonequilibriumness of a particle distribution as the resource. This was recently shown in Refs. [18, 19], where the nonequilibrium resource alone is used to fuel a refrigerator. An interesting device that has the capability of exploting such nonequilibriumness to produce power is the hot-carrier solar cell [20], which proposes to improve solar cells performance by exploiting high-energy (hot) carriers. In such a device the fast carrier extraction allows to exploit a nonthermal particle distribution to drive a charge current, and, consequenly, produce power. Additionally, with a slower extraction the particle distribution thermalizes and the efficacy of nonequilibrium can be tested.

Another consequence of out-of-equilibrium is the rise of additional noise, called shot noise. Usually, noise is considered detrimental because it hinders the accuracy of the device. However, fluctuations can reveal additional insight into the system considered, and therefore are worth studying and measuring. In particular, shot noise observations are not only used to characterize the conductance of mesoscopic conductors [21], but have also allowed to observe physical phenomena, like the fractional quantum Hall effect [22, 23]. Additionally, fluctuations play a crucial role in both stochastic and quantum thermodynamics, in which the randomness of observation outcomes is an important feature. These fields have attracted increasing interest in the last decades thanks to the technological developments in nanotechnology, which provides an experimental testing ground for the theory. In particular, the role of fluctuations is currently being investigated to establish fluctuation relations out of equilibrium, thermodynamic uncertainty relations, and connections to information.

While all the appended papers concern electronic mesoscopic systems out of equilibrium, papers [I] and [II] contribute to the research towards fluctuations, whereas paper [III] does it towards thermoelectric mesoscopic devices and nonequilibriumness as a resource. Specifically, in [I] and [II] the shot noise in the absence of currents is considered. This kind of noise was dubbed *delta-T* noise for its emergence when establishing a temperature bias, and was recently measured for the first time in Ref. [24]. While this experimental result paves the way for future measurements, the theoretical work in paper [I] studies the properties of such noise on both charge and heat currents. In particular, paper [I] analyzes both shot and thermal noises and their relation, proving a bound between them. Paper [II] extends the results of paper [I] providing a more detailed description of the noises, and extending the results to the finite-frequency noise and spin transport. Therefore, papers [I] and [II] motivate further endeavors to experimentally test the theoretical results and further studies on *delta-T* noise to investigate its properties and connections to information. Instead, paper [III] proposes a quantum transport model to describe the performance of hot-carrier solar cells. Recently, proofs of concept experiments on such devices have been realized using nanowires [25–29]. However, the theoretical characterization of the devices is often limited by the complexity of the underlying processes. The model introduced in paper [III] provides a simple description by focusing on the main properties of the involved processes. In this way, the model allows us to describe power production out of

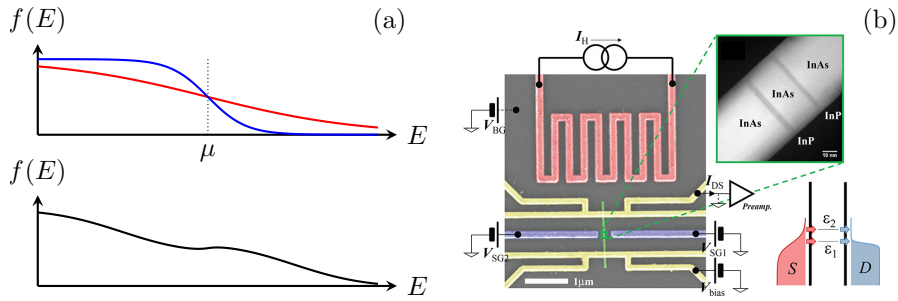

Figure 1.1: **(a)**: Examples of equilibrium (top panel) and nonequilibrium (bottom panel) probability distributions. The equilibrium distributions have well-defined chemical potential μ and temperature, hot (red) or cold (blue). Instead, the nonequilibrium distribution does not. **(b)**: Example of device locally at equilibrium. The heater (red) establishes a temperature difference between the ends of the nanowire (green). This out-of-equilibrium condition generates electric current through the nanowire. **Source**: [30].

a nonequilibrium distribution, and provides a thermodynamic characterization of the device. In particular, the latter shows that the hot-carrier solar cell is a bridge between the fields of thermoelectrics and photovoltaics. Paper [III] provides guidelines to improve the performance of hot-carrier solar cells in their realization. However, further studies are required for the model to effectively reproduce experiments.

1.1 Equilibrium and out-of-equilibrium systems

In order to discuss systems out of equilibrium, we first need to define what equilibrium is and how systems at equilibrium are characterized. Equilibrium represents the lack of information on a system [31]. In particular, the equilibrium state is described by the least-assuming probability distribution, namely the distribution that maximizes the entropy under some constraints. Such constraints depend on what quantities of the considered system are allowed to fluctuate around their average, and determine the *ensemble* used to describe the system. The ensemble in which both energy and number of particles can fluctuate is the grand-canonical ensemble, in which the system exhibits well-defined temperature T and chemical potential μ. Additionally, when the system is comprised of fermions, such as electrons, the Pauli exclusion principle allows to determine the occupation probability of each quantum state. This probability is given by the Fermi distribution, namely

$$f(E) = \frac{1}{1 + \exp[(E - \mu)/k_{\mathrm{B}}T]}, \tag{1.1}$$

illustrated in Fig. 1.1(a), and where k_{B} is the Boltzmann constant. Whenever an electronic system is not described by a unique Fermi distribution we say that

the system is out of equilibrium. In many experiments the out-of-equilibrium regime is reached by having two sides of the system at different temperatures and chemical potentials. This means that, while each side is locally at equilibrium, the global system is not. Indeed, there are no unique temperature and chemical potential describing the distribution of the whole system. An example of this kind of setup is illustrated in Fig. 1.1(b): the two sides of the device have different temperatures and chemical potentials thanks to the local heating and voltage bias applied. These sides act as electronic *reservoirs*, namely systems at equilibrium with large heat capacitance, such that their temperatures are virtually unaffected by the transport. In the example above, transport is made possible by a nanowire heterostructure connecting the electronic reservoirs. Nonetheless, there are many other stuctures that can make transport happen, for instance quantum point contacts [32], quantum dots [30, 33], or even molecules [34]. Since controlling chemical potentials and temperatures is experimentally feasible, many experiments investigate the *thermoelectric* properties of these different structures, which can then be implemented in thermometry, heat management, and work production. In Chapter 3 we will discuss thermoelectric devices in more detail. By contrast, out-of-equilibrium systems which exploit *nonequilibrium* probability distributions, namely local distributions different from the equilibrium one, are more difficult to approach both experimentally and theoretically. In fact, it is much harder to characterize and measure a nonequilibrium distribution compared to an equilibrium one. However, this kind of distribution can provide additional resources to perform useful tasks due to the entropy difference between the nonequilibrium distribution and the equilibrium one.

While papers [I] and [II] study the role of fluctuations in devices comprised of two reservoirs in different equilibrium states, paper [III] investigates the effect of nonequilibrium distributions on the performance of hot-carrier solar cell. In fact, even though such distributions are more challenging to study, they can often appear in transient dynamics or in regions between equilibrium distributions. This is the case in hot-carrier solar cells, where the carrier distribution is highly nonthermal when the carrier extraction is fast. Thus, such a nonequilibrium resource can be exploited to further improve the performance of the device.

1.2 Fluctuations

In classical macroscopic thermodynamics fluctuations are often neglected because their relative strength decreases with the number of elements N in the system, namely, for an observable O, $\langle \Delta O^2 \rangle / \langle O \rangle^2 \sim N^{-1/2}$. In mesoscopic systems this is not the case, and fluctuations can reveal additional insights on the physics of the system. A seminal result on fluctuations was the Nyquist-Johnson noise[35, 36], which relates the charge current fluctuations to the temperature of the sample. This relation is an early example of the fluctuation-dissipation theorem [37], which was further generalized in the Green-Kubo relations [38, 39] between correlations and transport coefficients. While these results are fundamental in the study of fluctuations, they are valid only for systems close

to equilibrium. In fact, in out-of-equilibrium systems such relations do not generally hold, and fluctuations have much richer features. For example, in the field of stochastic thermodynamics, fluctuation theorems [40–43] play a crucial role in the description of nonequilibrium systems and their entropy, and were instrumental for establishing the thermodynamic uncertainty relations [44–47]. Additionally, the out-of-equilibrium fluctuations have also proved to be useful in characterizing mesoscopic conductors. Indeed, while at equilibrium the noise is induced by the the randomness of the thermal excitation, hence called thermal noise, a different kind of noise emerges out of equilibrium. This noise is called shot noise (or partition noise) and originates from the discreteness of the transported particles. Apart from characterizing nanoscopic conductors [21], shot noise has been used in the detection of fractional charges [22, 23], Cooper pairs [48, 49], Bogoliubov quasiparticles [50], as well as in thermometry [51, 52] and quantum tomography [53–55].

While paper [III] focuses on the average currents, papers [I] and [II] are centered around the *delta-T* noise. This kind of noise is named after the temperature bias applied in the absence of a voltage bias which produced the fluctuations. However, it was first measured in electron-hole symmetric systems [24, 56, 57], in which the absence of a voltage bias corresponds to a vanishing average charge current. Thus, a general extension of the *delta-T* noise that applies to any mesoscopic conductor is the noise in the absence of currents. This noise is particularly interesting because it is allows to detect out-of-equilibrium conditions which maintain zero average current, as happens at equilibrium. Moreover, the fluctuations in absence of current were shown to satisfy the fluctuation-dissipation theorem in systems obeying the local detailed balance [58]. Therefore, this kind of noise may be used to test the fluctuation-dissipation theorem and possibly extend it to out-of-equilibrium conditions.

1.3 Thesis outline

Having discussed the general context and motivations behind the appended papers, the thesis now delves into the theoretical background necessary to understand these papers. The thesis is structured as follows.

First, in Chapter 2, we provide a brief introduction to the scattering theory, which is the theorical toolbox used in the appended papers. Here, we define the transport quantities and techniques of interest in the remainder of the thesis.

Next, in Chapter 3, we discuss a wide class of systems that are under the scope of the appeded papers: thermoelectric devices. These devices are also realized at the nanoscale and at low temperatures, where quantum mechanics determines their transport properties. In this chapter we also introduce the hot-carrier solar cell, a device in which the thermoelectric and photovoltaic effect are combined. This device is investigated in paper [III], and in Sec. 3.3 we discuss the novel transport model used in that paper to describe the device.

While Chapter 3 focuses on the average currents flowing in thermoelectric devices, Chapter 4 discusses the current fluctuations. In particular, we introduce

the *delta-T* noise and generalize it to the noise in absence of currents, both of which are investigated in papers [I] and [II].

In Chapter 5 we gather the main findings of the appended papers. The conclusions are drawn in Chapter 6.

Chapter 2

Scattering theory

This chapter is dedicated to the theoretical formalism used in the appended papers to describe transport, namely scattering theory. This simple approach to transport was introduced by Landauer and Büttiker in Refs. [59–61], and has proven to accurately predict and model many experiments [62–65]. The scattering theory is appropriate to describe systems in which the electron coherence length is large compared to the size of the device, such that electrons propagate obeying the laws of quantum mechanics. Additionally, scattering theory describes transport when electron-electron interactions are negligibly small or described at mean-field level. This allows to consider single-particle wavefunctions on a potential landscape.

2.1 Setup, scattering matrix and field operator

The setup considered is made of a central conductor, where the scattering takes place, which is connected to the reservoirs (labeled with greek letters) through one-dimensional leads. Here, we consider only stationary systems. The time-dependent case can be found in Ref. [66]. We approximate the leads to be semi-infinite, such that the particles propagating far from the conductor are described by plane-waves, as illustrated in Fig. 2.1. Additionally, the leads have multiple propagating modes, or *channels* (labeled with roman letters). Then, given an incoming particle wavepacket propagating from reservoir α to the conductor, we can decompose it into the othogonal basis of waves $e^{-ik(E)x}$ with coefficients $a_{\alpha i}(E)$. Similarly, we decompose the outgoing wavefunction propagating in the opposite direction, namely from the conductor to reservoir α, using the waves $e^{ik(E)x}$ with coefficients $b_{\alpha j}(E)$. The evolution that maps the incoming particle into the outgoing one is determined by the Schrödinger equation. Moreover, the linearity of the Schrödinger equation implies that the incoming ($a_{\alpha i}(E)$) and outgoing ($b_{\beta j}(E)$) coefficients are related through the *scattering matrix* $s_{\alpha i,\beta j}(E)$,

$$b_{\alpha i}(E) = \sum_{\beta j} s_{\alpha i,\beta j}(E) a_{\beta j}(E). \tag{2.1}$$

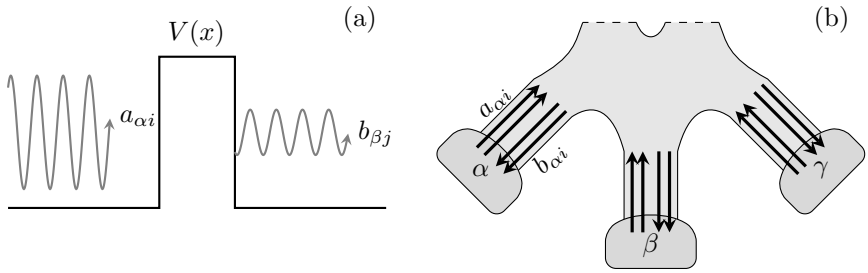

Figure 2.1: **(a)**: One-dimensional scattering problem. The incoming wavefunction $a_{\alpha i}$ scatters onto the potential barrier $V(x)$, leading to a transmitted wavefunction $b_{\beta j}$ and a reflected one (not drawn). The different amplitudes relate to the to the transmission probability of the barrier. **(b)**: General multi-terminal scattering setup. The reservoirs (greek letters) are connected to the conductor through one-dimensional leads having multiple channels (roman letters). The incoming (outgoing) particles from (to) reservoir α have amplitude $a_{\alpha i}$ ($b_{\beta j}$).

The scattering matrix cannot be an arbitrary matrix. In fact, imposing the conservation of particles during the scattering one finds that the scattering matrix $s(E)$ is unitary, namely $s^\dagger(E)s(E) = \mathbb{1}$, $\mathbb{1}$ being the identity matrix. Additionally, if the system is also invariant under time-reversal, the scattering matrix is symmetric.

The scattering matrix is the key to calculating transport quantities because it contains the transmission and reflection amplitudes across the conductor. However, in order to calculate the currents flowing in the system, we first need to formulate the corresponding quantum-mechanical operators. To do so, we use the canonical quantization procedure to obtain the quantum field associated with the particle. This allows us to write the currents flowing in the system in terms of such field, thereby obtaining a quantum description of the current. First, we expand the wavefunction into the orthogonal basis of propagating waves, $\exp(-iEt/\hbar \pm ik(E)x)$, and the orthonormal basis of transverse bound states $\chi_{\alpha i}(E, r_\perp)$. The former describes particles traveling between the reservoir and the central region, whereas the latter describes the channel in which the particle is propagating. The corresponding Fourier coeffients of the expansion, $a_{\alpha i}(E)$ and $b_{\alpha i}(E)$, are promoted to ladder operators, indicated with the hat $\hat{\bullet}$, and satisfy the canonical anti-commutation relations necessary for fermionic particles, namely

$$\{\hat{a}_{\alpha i}(E), \hat{a}_{\beta j}(E')\} = 0, \quad \left\{\hat{a}_{\alpha i}(E), \hat{a}^\dagger_{\beta j}(E')\right\} = \delta_{\alpha\beta}\delta_{ij}\delta(E - E'), \tag{2.2}$$

and similarly for $\hat{b}_{\beta j}(E)$. Then, the field operator of particles moving from and into reservoir α reads

$$\Psi_\alpha(\boldsymbol{r}, t) \equiv \sum_i \int dE e^{-iEt/\hbar} \frac{\chi_{\alpha i}(E, r_\perp)}{\sqrt{hv(E)}} \left[\hat{a}_{\alpha i}(E)e^{-ik(E)x} + \hat{b}_{\alpha i}(E)e^{ik(E)x}\right], \tag{2.3}$$

in which we used the unit-flux normalization by including the particle velocity $mv(E) = \hbar k(E)$. The summation runs over the open channels of the lead connecting to reservoir α.

2.2 Current operators

Using the field operator in Eq. (2.3) we calculate the current operators. Here, we provide the operators corresponding to the charge, $\hat{I}_\alpha(t)$ and the energy current, $\hat{I}^{(\mathrm{E})}_\alpha(t)$. Indeed, such currents are crucial in the study of most electronic mesoscopic systems. Additionally, when the reservoir α is a thermal bath, namely is described by a thermal distribution at temperature T_α and chemical potential μ_α, the first law of thermodynamics allows us to write the average entropy production in reservoir α as

$$T_\alpha \dot{S}_\alpha = \langle \hat{J}_\alpha(t) \rangle \equiv \langle \hat{I}^{(\mathrm{E})}_\alpha(t) - \mu_\alpha \hat{I}^{(\mathrm{N})}_\alpha(t) \rangle, \tag{2.4}$$

where $\hat{J}_\alpha(t)$ is the heat current, whereas $\hat{I}^{(\mathrm{N})}_\alpha(t)$ is the particle current. In particular, the latter is related to the charge current via the particle charge q as $\hat{I}_\alpha(t) = q\hat{I}^{(\mathrm{N})}_\alpha(t)$. Additionally, other kinds of currents, for instance spin currents, can be calculated in a similar fashion. In particular, for spin transport it is possible to include the spin indices into the reservoir indices.

To calculate the current operators (see App. A for details), we consider the case in which the energy scale of the transport, which typically is on the order of the applied external biases, for instance the voltage bias, is much smaller than the Fermi energy μ_0 of the system, namely

$$|E - E'| \ll E \sim \mu_0. \tag{2.5}$$

This means that the the energy dependencies of wavenumber $k(E)$, particle velocity $v(E)$, and transverse modes $\chi_{\alpha i}(E)$ are weak compared to the energy-scale of the transport, and we can thus approximate $k(E) \approx k(E'), v(E) \approx v(E'), \chi_{\alpha i}(E, r_\perp) \approx \chi_{\alpha i}(E', r_\perp)$. This allows one to write the charge current operator flowing into the reservoir α as

$$\hat{I}_\alpha(t) = \frac{q}{h} \sum_i \int dE dE' e^{-i(E-E')t/\hbar} \left[\hat{b}^\dagger_{\alpha i}(E') \hat{b}_{\alpha i}(E) - \hat{a}^\dagger_{\alpha i}(E') \hat{a}_{\alpha i}(E) \right], \tag{2.6}$$

where q is the electric charge of the considered fermions, specifically $q = -e$ for electrons. Similarly, the energy current operator is

$$\hat{I}^{(\mathrm{E})}_\alpha(t) = \frac{1}{h} \sum_i \int dE dE' \frac{E + E'}{2} e^{-i(E-E')t/\hbar} \left[\hat{b}^\dagger_{\alpha i}(E') \hat{b}_{\alpha i}(E) - \hat{a}^\dagger_{\alpha i}(E') \hat{a}_{\alpha i}(E) \right]. \tag{2.7}$$

As expected, the currents flowing into reservoirs α account for the transferred quantity, charge and energy respectively, at all energies and in all channels i. Additionally, it is clear from Eqs. (2.6) and (2.7) that the particles propagating towards the reservoir (corresponding to the operators $\hat{b}_{\alpha i}(E)$) increase the

currents, whereas the particles escaping the reservoir (corresponding to the operators $\hat{a}_{\alpha i}(E)$) decrease it. However, the particles propagating towards the reservoir have been subjected to a scattering process in the conductor. Thus, the operators $\hat{b}_{\alpha i}(E)$ are related to the operators $\hat{a}_{\alpha i}(E)$, and this relation is governed by the scattering matrix through Eq. (2.1). Substituting this linear relation in the charge current operator of Eq. (2.6), we obtain

$$\hat{I}_\alpha(t) = \frac{q}{h}\sum_i \int dE dE' e^{-i(E-E')t/\hbar} \mathcal{A}^{E',E}_{\alpha i,\beta j,\gamma k} \hat{a}^\dagger_{\beta j}(E')\hat{a}_{\gamma k}(E) \tag{2.8}$$

where the summation over the repeated indices βj and γk is understood and the tensor in the integral is defined as

$$\mathcal{A}^{E',E}_{\alpha i,\beta j,\gamma k} \equiv s^*_{\alpha i,\beta j}(E')s_{\alpha i,\gamma k}(E) - \delta_{\alpha i,\beta j}\delta_{\alpha i,\gamma k}, \tag{2.9}$$

and contains all the information about the scattering process.

The currents in Eqs. (2.6), (2.7) and (2.8) are still operators. However, in an experiment the actual measured currents will correspond to the spectrum of such operators, and clearly relevant quantities to characterize the system are the average currents flowing into the reservoirs. Such averages can be calculated in this framework by taking the expectation value of the ladder operators, resulting in

$$I_\alpha = \langle \hat{I}_\alpha(t)\rangle = \frac{q}{h}\sum_i\sum_{\beta j}\int dE D_{\alpha i,\beta j}(E)\left[f_\alpha(E) - f_\beta(E)\right], \tag{2.10}$$

$$I^{(\mathrm{E})}_\alpha = \langle \hat{I}^{(\mathrm{E})}_\alpha(t)\rangle = \frac{q}{h}\sum_i\sum_{\beta j}\int dE E D_{\alpha i,\beta j}(E)\left[f_\alpha(E) - f_\beta(E)\right], \tag{2.11}$$

where $D_{\alpha i,\beta j}(E) = |s_{\alpha i,\beta j}(E)|^2$ is the transmission probability from reservoir β and channel j to reservoir α and channel i, whereas the quantity $f_\alpha(E)$ is the occupation number at energy E of reservoir α. While the transmission probabilities depend on the properties of the scatterer, the occupation number is a *boundary condition* of the scattering theory formalism. Indeed, the reservoirs are often considered large enough that the transport through the conductor does not affect the particle distribution. Alternatively, the distribution in the reservoirs can be kept fixed by an external agent. A particular and often considered case is the one in which the reservoirs are thermal baths at temperature T_α and chemical potential μ_α. Then, the occupation number is given by the Fermi distribution,

$$f_\alpha(E) = \frac{1}{1+\exp\left[(E-\mu_\alpha)/k_\mathrm{B}T_\alpha\right]}. \tag{2.12}$$

2.3 Current fluctuations

While average currents are important to establish the performance of devices, the actual measuments will detect values fluctuating around such averages.

These fluctuations can also give insight on the device and characterize its performance, as discussed in Sec. 1.2. Here, we provide the procedure to follow in order to calculate current fluctuations in the scattering formalism, focusing on the charge current fluctuations. Other current fluctuations can be obtained in a similar fashion. In Chapter 4 we will consider in more detail the current fluctuations investigated in papers [I] and [II], especially regarding heat and spin current fluctuations.

To study the current fluctuations, the *symmetrized* noise is often used. In particular, for charge current fluctuations it is defined through the deviation from the mean $\Delta\hat{I}_\alpha(t) = \hat{I}_\alpha(t) - \langle\hat{I}_\alpha(t)\rangle$ as

$$S^I_{\alpha\beta}(t-t') \equiv \langle\Delta\hat{I}_\alpha(t)\Delta\hat{I}_\beta(t') + \Delta\hat{I}_\beta(t')\Delta\hat{I}_\alpha(t)\rangle, \tag{2.13}$$

and analogously for other types of currents. Taking the Fourier transform we analyze the finite-frequency components of the symmetrized charge noise, obtaining

$$2\pi\delta(\omega+\omega')S^I_{\alpha\beta}(\omega) = \langle\Delta\hat{I}_\alpha(\omega)\Delta\hat{I}_\beta(\omega') + \Delta\hat{I}_\beta(\omega')\Delta\hat{I}_\alpha(\omega)\rangle. \tag{2.14}$$

Now, we use the following relation on the expectation values of fermionic ladder operators

$$\langle\hat{a}_1^\dagger\hat{a}_2\hat{a}_3^\dagger\hat{a}_4\rangle = \langle\hat{a}_1^\dagger\hat{a}_2\rangle\langle\hat{a}_3^\dagger\hat{a}_4\rangle + \langle\hat{a}_1^\dagger\hat{a}_4\rangle\langle\hat{a}_2\hat{a}_3^\dagger\rangle, \tag{2.15}$$

to calculate the current correlators in Eq. (2.14). Here, we show the result of such a calculation for the current auto-correlator $\langle\hat{I}_\alpha(\omega)\hat{I}_\alpha(\omega')\rangle$, given by

$$\begin{aligned}\langle\hat{I}_\alpha(\omega)\hat{I}_\alpha(\omega')\rangle &= 4\pi^2\delta(\omega)\delta(\omega')\langle\hat{I}_\alpha(t)\rangle^2 + \\ &+ \delta(\omega+\omega')\frac{q^2}{\hbar}\sum_{i,i'}\int dE\mathcal{A}^{E,E+\hbar\omega}_{\alpha i,\beta j,\gamma k}\mathcal{A}^{E+\hbar\omega,E}_{\alpha i',\gamma k,\beta j}f_\beta(E)\left[1-f_\gamma(E+\hbar\omega)\right].\end{aligned} \tag{2.16}$$

The first term on the right-hand side corresponds to the product of the averages $\langle\hat{I}_\alpha(\omega)\rangle\langle\hat{I}_\alpha(\omega')\rangle$ and thus cancels out when calculating the noise. Instead, the second term constitutes the noise. In particular, the term $f_\beta(E)[1-f_\gamma(E+\hbar\omega)]$ suggests that the incoming particle absorbed a quantum of energy $\hbar\omega$ during the scattering, thereby we refer to the noise generated by this current correlator as *absorption* noise, $S^-_{\alpha\alpha}(\omega)$. By contrast, the current correlator $\langle\hat{I}_\alpha(\omega')\hat{I}_\alpha(\omega)\rangle$ contributes to the noise with an analogous integral containing $f_\beta(E+\hbar\omega)\left[1-f_\gamma(E)\right]$, which suggests that the incoming particle emitted a quantum of energy $\hbar\omega$. Thus, we refer to the noise generated by this correlator as *emission* noise, $S^+_{\alpha\alpha}(\omega)$. These two noise contributions read

$$S^-_{\alpha\alpha}(\omega) = \frac{q^2}{h}\sum_{i,i'}\int dE\mathcal{A}^{E,E+\hbar\omega}_{\alpha i,\beta j,\gamma k}\mathcal{A}^{E+\hbar\omega,E}_{\alpha i',\gamma k,\beta j}f_\beta(E)\left[1-f_\gamma(E+\hbar\omega)\right], \tag{2.17}$$

$$S^+_{\alpha\alpha}(\omega) = \frac{q^2}{h}\sum_{i,i'}\int dE\mathcal{A}^{E+\hbar\omega,E}_{\alpha i,\beta j,\gamma k}\mathcal{A}^{E,E+\hbar\omega}_{\alpha i',\gamma k,\beta j}f_\beta(E+\hbar\omega)\left[1-f_\gamma(E)\right], \tag{2.18}$$

where the summation over the indices βj and γk is understood. As expected, the two noise contributions coincide at zero frequency, $\hbar\omega = 0$, where the

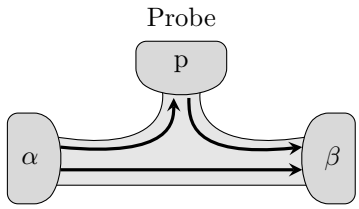

Figure 2.2: Two-reservoirs system connected to a probe. The distribution of particles inside the probe is determined by imposing constraints on the currents flowing into it. When particles travel from α to β passing through the probe coherence is (partially) lost.

distinction between emission and absorption is meaningless. An analogous calculation can be performed for the current cross-correlators $\langle \hat{I}_\alpha(\omega)\hat{I}_\beta(\omega')\rangle$. Furthermore, the symmetrized noise entering Eq. (2.14) is simply the sum of emission and absorption noise, $S^I_{\alpha\beta}(\omega) = S^+_{\alpha\beta}(\omega) + S^-_{\alpha\beta}(\omega)$. Even though the symmetrized noise is widely investigated both theoretically and experimentally, the measured finite-frequncy noise depends on the detection scheme and can take on non-symmetric combinations of absorption and emission noise [67, 68].

While this section provided the general formulations and derivations of noise in the context of the scattering formalism, in Chapter 4 these notions will be applied to specific and experimentally feasible scenarios that are investigated in papers [I] and [II], and the distinction between shot and thermal noise will be discussed.

2.4 Büttiker and dephasing probes

The scattering theory discussed so far describes perfectly coherent transport in a mesoscopic conductor. However, in a realistic setting, scattering with impurities and interactions introduces incoherent or inelastic elements to the scattering. To capture these phenomena and investigate their effect on the transport, *Büttiker* and *dephasing probes* [69–73] are often used in mesoscopic physics. These probes are additional elements in the scattering framework, as illustrated in Fig. 2.2. However, unlike the reservoirs, the probe's particle distribution is not a boundary condition of the scattering problem but is determined by imposing constraints on the currents flowing into the probe. The imposed constraints govern the nature and properties of the probe. Büttiker probes can be both conceptual tools used to model particular processes or real, physical components used in experiments. The latter usually consist of large metallic contacts attached to the mesoscopic conductor which are left floating or are connected to a voltmeter, namely the charge current flowing into them is ideally zero. Büttiker probes are often considered to have an efficient thermalization, such that their particle distribution is thermal. The chemical potential (or equivalently the voltage) and temperature of the probe's distribution are determined by imposing vanishing particle current, $I^{(\mathrm{N})}_\alpha = I_\alpha/q$,

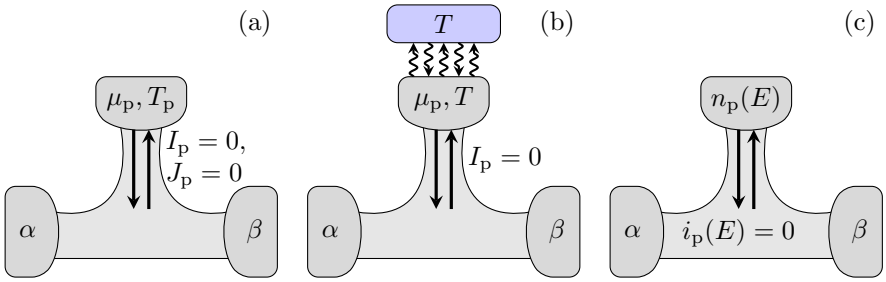

Figure 2.3: Diagrams of Büttiker and dephasing probes and their constraints on the current flows. **(a)**: Büttiker probe described by a thermal distributrion of chemical potential μ_p and temperature T_p obtained by imposing zero charge and heat currents into the probe. **(b)**: Pure voltage probe, namely a Büttiker probe connected to the environment (blue) at temperature T. The heat flow into the probe is dominated by the flow between probe and environment, hence the probe's temperature corresponds to T. **(c)**: Dephasing probe whose distribution $n_\mathrm{p}(E)$ is determined by imposing zero current at each energy, $i_\mathrm{p}(E) = 0$.

and heat current into the probe, namely

$$I_\mathrm{p}^{(\mathrm{N})} = 0, \quad J_\mathrm{p} = 0 \quad \Rightarrow \quad I_\mathrm{p}^{(\mathrm{E})} = 0, \tag{2.19}$$

as depicted in Fig. 2.3(a). Indeed, if we imagine a situation in which the probe has a chemical potential μ_p that allows a net particle flow into the probe itself, the probe distribution is not stationary and needs to change because of the inflow of particles, establishing a higher chemical potential. The opposite happens if the chemical potential μ_p allows a net particle flow out of the probe. Thus, the stationary condition is reached when the average particle current is zero. The same argument applies for the heat flow. A particular instance of a Büttiker probe happens when the thermal conductance between the probe and the environment is large. In this case, the heat exchange between the probe and the other reservoirs is negligible compared to the heat flow to the environment, and consequently the probe's temperature coincides with the environment's temperature, as shown in Fig. 2.3(b). Thus, only the probe's chemical potential is affected by the transport towards the other terminal, and we refer to the probe as a pure *voltage* probe.

Since the distribution of the particles flowing into the Büttiker probe is changed into the probe's thermal distribution, the Büttiker probes add inelastic scattering to the framework of scattering theory. Additionally, when a particle exits the Büttiker probe, its phase is reset and carries no correlation with the phase the particle had before entering the probe. Therefore, the Büttiker probe also includes decoherence.

Another kind of probe is the dephasing probe, illustrated in Fig. 2.3(c). Unlike the Büttiker probe, the dephasing probe does not have a physical implementation, but is only a conceptual tool. This stems from the constraint on the current flow required for this kind of probe. In fact, the dephasing

probe requires the particle flow at each energy to vanish, namely, defining the energy-resolved current into the probe $i_{\mathrm{p}}(E)$ through the integral

$$I_{\mathrm{p}} \equiv \int dE i_{\mathrm{p}}(E), \tag{2.20}$$

the dephasing probe requires

$$i_{\mathrm{p}}(E) = 0. \tag{2.21}$$

This condition is clearly much stronger than those of Eq. (2.19), and in fact the probe distribution $n_{\mathrm{p}}(E)$ which satisfies the condition is generally a nonequilibrium distribution. Since the dephasing probe does not reorganize the particle distribution, the energy of a particle escaping the probe is equal to the energy the particle had when it entered the probe. However, the particle's phase is reset. Therefore, the dephasing probe is a tool to introduce elastic decoherence to the scattering framework.

In conclusion, probes are useful tools to include inelastic or elastic decoherence in the scattering theory of transport. Paper [III] makes use of such tools, specifically of Büttiker probes, to describe the processes of carrier thermalization and carrier relaxation in a hot-carrier solar cell. These processes are mediated by carrier-carrier and carrier-phonon interaction, respectively, which are not included in the basic scattering formalism introduced in Sec. 2.1. However, the use of Büttiker probes allows us to mimic their effects and include them in the scattering description of the device.

Chapter 3

Thermoelectric devices

In this chapter a brief overview of thermoelectric devices is presented. Here, we discuss the difference between classical and quantum thermoelectrics, as well as introduce the setups considered in the appended papers. These consist of quantum thermoelectric heat engines and hot-carrier solar cells, whose descriptions are based on the scattering theory discussed in the previous chapter. The transport quantities obtained with such a formalism allow to characterize and quantify the performance of the devices both in linear and, most importantly, nonlinear response.

3.1 Classical and quantum thermoelectrics

After the discovery of the Seebeck [74] and Peltier [75] effects, which make use of temperature differences to induce charge currents and vice-versa, thermoelectric materials have been used in heat control, heat to work conversion and refrigeration [76]. In particular, classical thermoelectric materials are characterized by a thermalization length $\ell_{\rm th}$ smaller than the typical size of

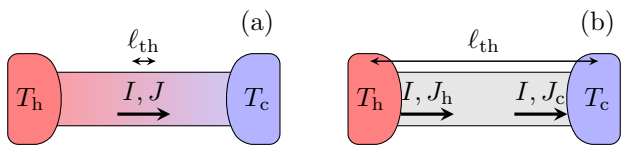

Figure 3.1: **(a)**: Classical thermoelectrics. The thermalization length $\ell_{\rm th}$ is the smallest scale of the system. Thus, the electrons in the thermoelectric structure are locally at equilibrium, and their temperature varies smoothly between the hot temperature $T_{\rm h}$ and the cold one $T_{\rm c}$. Electric and heat flows, I and J, can be described locally by the Boltzmann equation. **(b)**: Quantum thermoelectrics. The size of the thermoelectric structure is smaller than the thermalization length, and quantum effects occur in it. Current flows need to be calculated accounting for the whole system.

the material, as illustrated in Fig. 3.1(a). In this case the electrons along the material are locally at equilibrium, meaning that their local distribution is a thermal distribution characterized by smoothly varying chemical potential and temperature, and they are well described by the Boltzmann equation [77]. Recently, the technological advances in nanotechnology and refrigeration have made possible the realization of structures with a typical size smaller than the thermalization length [78]. Indeed, it is now possible to fabricate structures with typical size on the order of 10 nm, and the low temperatures reached in many experiments weaken the strength of electron-electron and electron-phonon interactions [3, 79], thereby increasing the thermalization length to many micrometers. Consequently, the behavior of such structures is influenced by quantum phenomena like tunneling and interference, and we refer to them as quantum thermoelectrics [4]. Since in quantum thermoelectrics the scale of thermalization is larger than the size of the thermoelectric structure, there is no local equilibrium, as shown in Fig. 3.1(b), and one must consider the whole system to characterize the device. The study of quantum thermoelectrics allows to design novel devices that exploit the quantum effects happening in them, as well as explore new aspects of thermodynamics at the nanoscale, where it coexists with quantum mechanics [80, 81]. Indeed, thermoelectricity is used as a mean to study the state of nanostructures by observing its response to external temperature and voltage biases [82]. Additionally, the small size of quantum thermoelectrics would be excellent for local operation, like on-chip refrigeration and heat management.

Since the appended papers are centered around quantum thermoelectrics, in the following we will focus only on them and disregard the classical thermoelectrics. In particular, papers [I] and [II] investigate fluctuations in the absence of currents. This condition is for instance reached in thermoelectric heat engines when they are operating at the thermovoltage, namely the voltage at which the power output of the device vanishes. Instead, paper [III] revolves around the hot-carrier solar cell, which is a device combining the benefits of thermoelectrics and photovoltaics.

3.2 Thermoelectric heat engine

Since the Seebeck effect allows to drive a charge current from a temperature difference, it is natural to consider a device in which such effect is used to produce power. This device is the thermoelectric heat engine [84–86]. Here, we consider steady-state quantum thermoelectric heat engines where local interactions can be neglected, such that the scattering theory description applies. A typical two-terminal device is illustrated in Fig. 3.2(a), where left (L) and right (R) reservoirs are kept at different temperatures and chemical potentials. In particular, the left reservoir is hotter than the right one, namely $T_{\mathrm{L}} > T_{\mathrm{R}}$, but has lower chemical potential $\mu_{\mathrm{L}} < \mu_{\mathrm{R}}$. Importantly, the two reservoirs are connected by a conductor of energy-dependent transmission probability $D(E)$, which acts as an energy filter. Here, for simplicity, we consider only the single-channel case, but these considerations can be easily

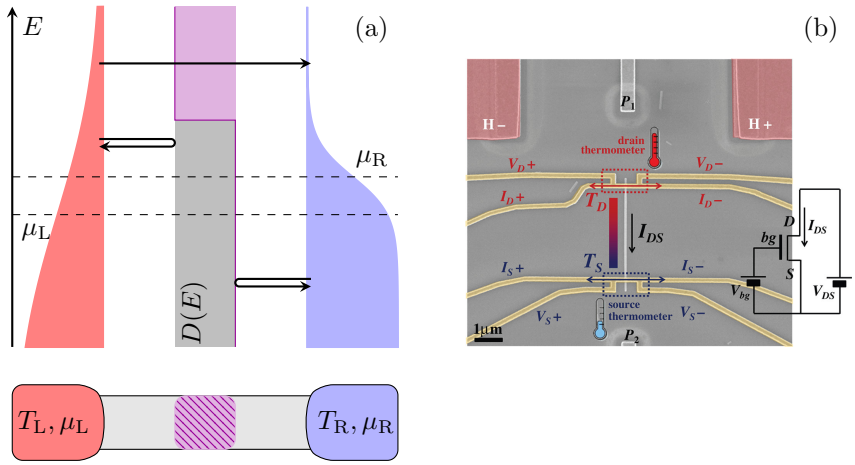

Figure 3.2: **(a)**: Energy diagram of a quantum thermoelecric heat engine. The transmission probability of the scatterer $D(E)$ acts as an energy filter allowing only high-energy electrons to tunnel. Combined with the temperature difference of the reservoirs, this allows to drive a charge current against a voltage bias, thereby producing power. **(b)**: Scanning electron micrograph of a thermoelectric heat engine in which the reservoirs (yellow) are connected by a nanowire. **Source**: [83].

extended to multi-channel conductors. For example, when the transmission allows only electrons with energy larger than a threshold energy E_0 to be transmitted, namely

$$D(E) = \begin{cases} 1 & \text{if } E > E_0, \\ 0 & \text{otherwise,} \end{cases} \tag{3.1}$$

as depicted in Fig. 3.2(a), the temperature bias can generate a particle current against the chemical potential bias [32]. This makes the device generate power starting from a temperature difference, in analogy to the traditional heat engine. In particular, the power output of the device is determined by the product of the particle flow $I^{(\mathrm{N})} = I/q$ and the chemical potential difference, namely

$$P \equiv (\mu_\mathrm{R} - \mu_\mathrm{L})\, I^{(\mathrm{N})} = \Delta\mu I^{(\mathrm{N})}, \tag{3.2}$$

where the current is defined as positive when it flows from left to right. Since this power is generated only by using the heat resource, the traditional heat engine efficiency is defined as power divided by heat flow out of the hot reservoir, that we take here to be the left one without loss of generality. Such efficiency η is bounded by the Carnot efficiency, namely

$$\eta \equiv \frac{P}{J_L} \leq \eta^{\mathrm{Carnot}} \equiv 1 - \frac{T_\mathrm{R}}{T_\mathrm{L}}, \tag{3.3}$$

because of the second law of thermodynamics. Indeed, the inequality stems from the non-decrease of global entropy combined with energy conservation.

Since both power and efficiency crucially depend on the transmission probability $D(E)$ through the currents, see Eqs. (2.10) and (2.11), the characteristics of the conductor play a fundamental role in determining the performance of the device. To this end, different kinds of conductors have been studied and implemented to achieve different effects: For example, the transmission of (3.1) is approximated by the quantum point contact [32, 87], and was shown to maximize the efficiency of the thermoelectric heat engine while achieving the maximum power output [88, 89]. Instead, the resonant transmission of quantum dots also provides the thermoelectric effect [30, 33, 90], and allows heat engines to operate efficiently, albeit at reduced power output. Nonetheless quantum thermoelectric heat engines have been realized also with other kinds of structures, for instance nanowires [83, 91], as shown in Fig. 3.2(b).

In the study of transport in mesoscopic devices, and consequently of quantum thermoelectric heat engines, the linear response is often considered. In this regime, characterized by being close to the equilibrium condition, transport is described through the kinetic coefficients. These comprise the electrical and thermal conductance, G and K respectively, as well as the Seebeck and Peltier coefficients, S and Π respectively. Such quantities are the linear coefficients in the expansion around equilibrium, and are defined as

$$G \equiv \left.\frac{I}{\Delta V}\right|_{\Delta T=0}, \quad K \equiv \left.\frac{J_{\mathrm{L}}}{\Delta T}\right|_{I=0}, \quad S \equiv -\left.\frac{\Delta V}{\Delta T}\right|_{\Delta T=0}, \quad \Pi \equiv \left.\frac{J_{\mathrm{L}}}{I}\right|_{\Delta T=0}. \tag{3.4}$$

Additionally, they must satisfy the Onsager-Casimir relations [92, 93], which state the invariance under time-reversal of both electrical and thermal conductance, while relating the Seebeck and Peltier coefficients together. Such kinetic coefficients can be combined into the dimensionless figure of merit ZT, namely

$$ZT \equiv \frac{GS^2T}{K}, \tag{3.5}$$

which is a measure of efficiency in the linear response regime. However, beyond this regime the picture becomes more complicated. In fact, in out-of-equilibrium conditions both charge and heat currents are nonlinear functions of temperatures and chemical potentials, and screening effects take place [94, 95]. In such a case, the kinetic coefficients are not sufficient to give a complete description of the system. Additionally, the ZT figure of merit does not measure the thermodynamic efficiency any longer [96]. While the nonlinear regime is more complex, it allows to study out-of-equilibrium fluctuations as well as the impact of nonequilibrium distributions on the performance of devices. Both such aspects are considered in the appended papers. Therefore, in the following, we will not restrict the discussion to the linear response regime, but rather consider full nonlinear quantities. Specifically, in papers [I] and [II] the nonlinear fluctuations are investigated, whereas in paper [III] the nonlinear power and efficiency are used to characterize the device.

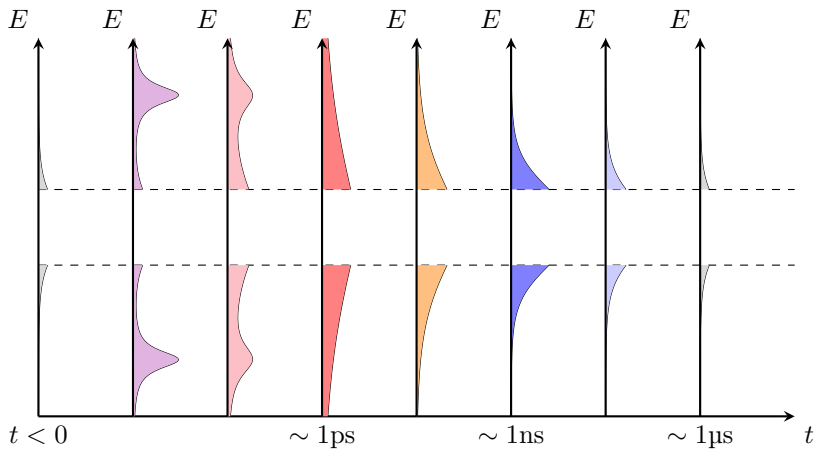

Figure 3.3: Schematic representation of the time-scales of the processes in a hot-carrier solar cell. The dashed lines delimit the absorber bandgap, whereas the coloured regions describe the carrier occupation probability. Before light absorption, the carrier distribution is at equilibrium with the environment at low temperature (gray), making the number of carriers small. The light absorption generates a strongly nonthermal distribution (purple), which thermalizes due to carrier-carrier interaction on the scale of 1 ps, resulting in a thermal distribution (red) at high temperature. The carrier-phonon scattering deplete the carrier excess energy, thereby cooling the carriers to the lattice temperature (blue) on the scale of 1 ns. The carrier recombination depletes the carriers on the scale of 1 µs, bringing them back to equilibrium with the environment. Depending on the time-scale of the carrier extraction, the device can be a hot-carrier solar cell (smaller than 1 ns), a solar cell (between 1 ns and 1 µs), or even not able to produce power (larger than 1 µs).

3.3 Hot-carrier solar cell

While heat engines use heat as the resource to produce power, conventional solar cells convert the electrochemical energy resulting from the generation of electron-hole pairs into power by separating the carriers. As suggested by the name, hot-carrier solar cells [20] have elements of both kinds of devices. Indeed, while the generation of electron-hole pairs by photon absorption is fundamental for the operation of the hot-carrier solar cell, the device does not wait for the electrochemical energy to be formed. In fact, in conventional solar cells this energy is established when the carriers relax to the lattice temperature by losing energy in the carrier-phonon scattering processes.

However, when the absorbed photon has energy larger than the bandgap E_G, the generated carriers have some excess energy. We call such carriers *hot-carriers* [97], and their excess energy is wasted as heat to the lattice in conventional solar cells. This loss limits notably the efficiency of solar cells [98]. The concept behind hot-carrier solar cells is to avoid such an energy loss and instead exploit the hot-carrier excess energy to improve the performance of the device.

This is made possible by the use of nanostructures in which the carrier extraction is faster than the relaxation, such that the hot-carrier excess energy is not completely wasted as heat to the lattice when the carrier is extracted and its energy is harvested. In particular, the typical time scale of the carrier relaxation to the lattice temperature depends on the specifics of the material, but is typically on the order of 1 ns [99, 100], as depicted in Fig. 3.3. Additionally, there are two more processes that crucially influence the distribution of carriers: the recombination and the thermalization. The recombination process depletes the number of carriers while emitting photons, therefore it is detrimental to both power production and efficiency. This process has typical time scale on the order of 1 µs, much slower than the relaxation time. In fact, conventional solar cells using diffusion to extract the carriers operate after the relaxation has taken place, but before the recombination comes into effect. By contrast, the carrier thermalization is typically on the order of 1 ps, thereby faster than the relaxation time. This process is mediated by carrier-carrier scattering processes and drives the carrier distribution towards a thermal distribution, with a temperature and chemical potential different from the ones established after the relaxation. Hot-carrier solar cells operate in the timeframe prior to the complete carrier relaxation.

In particular, if the extraction happens after the carrier thermalization, the hot-carrier solar cell uses both heat and chemical energy as resources thanks to the temperature and chemical potential of the hot-carriers. This clarifies the connection of hot-carrier solar cells to both heat engines and solar cells [101, 102]. Additionally, when the extraction is even faster than the carrier thermalization, the distribution of carriers is highly nonthermal and generally depends on both the light spectrum and the absorption properties of the material. In this case the device exploits a nonequilibrium distribution to produce power. Another similarity to heat engines is the use of energy filters, which is often considered in hot-carrier solar cells to select the high-energy

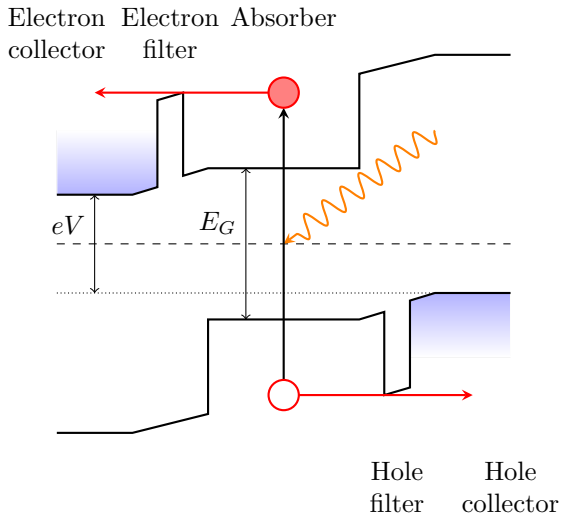

Figure 3.4: Schematic of the band diagram of a electron-hole symmetric hot-carrier solar cell. In the absorber region, of bandgap E_G an electron-hole pair is generated with the absorption of a photon (orange). When the photon energy is larger than E_G the generated carriers have extra energy (hot-carriers). The high-energy carriers are selected by energy filters, and electrons and holes are separated to the respective collectors, thereby generating an electric current against the voltage bias V.

carriers and avoid backflows from the collectors. A simple illustration of how a hot-carrier solar cell works is depicted in Fig. 3.4, in which the separation and the selection of high-energy carriers allows to drive a charge current against the voltage V, thereby producing power.

Efforts in realizing and testing experimentally such kind of devices were recently made [25–29, 103]. In particular, a realization of a hot-carrier solar cell is shown in Fig. 3.5, where nanoantennas are placed at a defined position on nanowires, concentrating light on the absorber region, while the energy filter is obtained by changing the material composing the nanowire to one with higher bandgap. The small size of the sample allows the fast extraction of the hot carriers through the energy filter, which yields a net charge current across the nanowire. This current allows the device to produce power and is determined by the distribution of hot carriers that is extracted. However, such a distribution is very difficult to determine because it heavily depends on the spectrum of impinging light, the absorption of the material used, as well as the carrier-carrier and carrier-phonon scattering which lead to carrier thermalization, relaxation to the lattice temperature and carrier recombination.

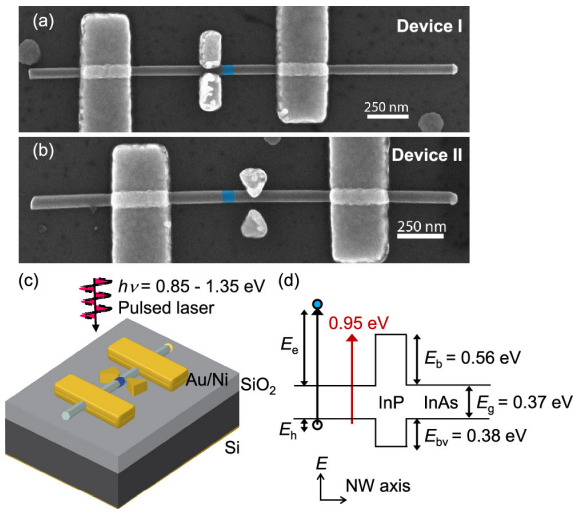

Figure 3.5: Experiment on a hot-carrier solar cell device based on InAs-InP-InAs nanowire heretostructures. **(a, b)**: Scanning electron micrographs of the devices with dipole nanoantenna (a) and bowtie nanoantenna (b). The InP region (blue) acts as an energy filter. **(c)**: Schematic illustration of the device. **(d)**: Schematic band diagram of the heterostructure. In this experiment the generated electron obtains most of the excess energy from the photon. **Source**: [26].

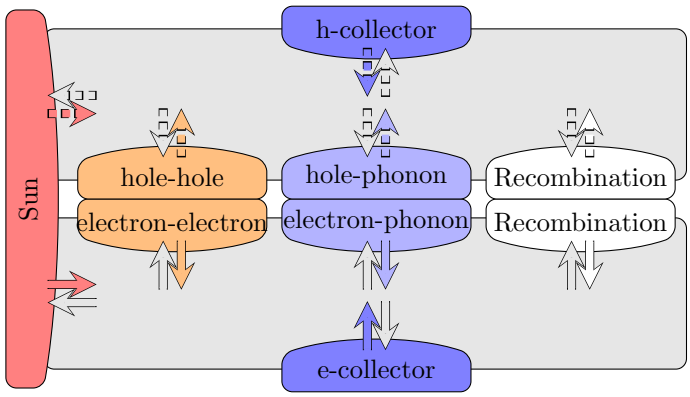

Figure 3.6: Diagram of the multi-probe model used to describe the hot-carrier solar cell. The electron-electron (hole-hole) and electron-phonon (hole-phonon) terminals are Büttiker probes accounting for carrier-carrier thermalization and relaxation to the lattice temperature respectively. The sun, recombination and collectors terminals are reservoirs accounting for the creation, the loss, and the extraction of carriers. The injected electrons (solid arrow) and holes (dashed arrows) can undergo thermalization, relaxation, recombination or be extracted to their collector with probabilities controlled by the transmissions $D_{\alpha,\beta}(E)$ and $D'_{\alpha\beta}(E)$, respectively. In the electron-hole symmetric case the top and bottom part of the diagram are equivalent, hence we focus only on the electron part.

3.3.1 Multi-probe model

Paper [III] approaches the task of modeling the hot-carrier distribution by studying the device under the scattering theory formalism and including the effects of carrier thermalization, relaxation and recombination through the use of Büttiker probes. To this end, a multi-probe model, illustrated in Fig. 3.6, is devised. The terminals we consider describe each a different process and thus have different characteristics. In particular, they comprise both thermal reservoirs and Büttiker probes, previously discussed in Sec. 2.4. Therefore, each terminal requires some description.

- *Collector reservoir* ($\alpha = \text{col}$) allows the extraction of carriers. In particular, the electron collector and the hole collector are distinct, such that a charge current is driven across the device, and electrical power can be produced. The collector distribution is considered to be thermal at fixed temperature T_{col} equal to the environment temperature. Instead, its chemical potential μ_{col} is controlled by an external voltage bias or is determined by a resistor characterizing the power production in a closed circuit.

- *Sun reservoir* ($\alpha = \text{sun}$) represents the quasiparticles created in the absorber via the absorption of sun photons. This reservoir makes the

device work providing the necessary *resources*. While the principle behind this terminal can be applied to any kind of light source, we focus on sunlight by considering the injection reservoir's distribution to be a thermal distribution of temperature T_{sun}, and zero chemical potential, $\mu_{\text{sun}} = 0$. Indeed, this distribution corresponds to the distribution of carriers at equilibrium with a photon bath at the same temperature.

- *Electron-electron probe* ($\alpha = \text{e-e}$) is a Büttiker probe modeling the electron-electron elastic scattering, in which both the total number of carriers and the total energy of the carriers are conserved, and that is responsible for the carrier thermalization. Since this process drives the carriers towards a thermal distribution, we characterize the thermalization probe by a thermal distribution of temperature $T_{\text{e-e}}$ and chemical potential $\mu_{\text{e-e}}$. These intensive properties are determined by imposing the Büttiker probe conditions on the flows into the probe, namely

$$I^{(\text{N})}_{\text{e-e}} = 0, \quad I^{(\text{E})}_{\text{e-e}} = 0. \tag{3.6}$$

  In particular, these conditions mirror the particle and energy conservation of the carrier-carrier elastic scattering.

- *Electron-phonon probe* ($\alpha = \text{e-ph}$) is a Büttiker probe modeling the electron-phonon scattering, in which the total number of carriers is conserved, while the total carrier energy is not. In fact, hot carriers lose their excess energy to the lattice through this mechanism, which causes the carrier distribution to relax to the lattice temperature. Thus, the relaxation probe is characterized by a thermal distribution in which the temperature is fixed to be the environment temperature, and coincides with the collector temperature, $T_{\text{e-ph}} = T_{\text{col}}$. Indeed, the interaction with the phonon lattice means that this probe is exchanging heat with that phonon bath, which dominates over the heat exchanged with the other terminals. This means that the relaxation probe is a pure voltage probe, whose chemical potential $\mu_{\text{e-ph}}$ is obtained by imposing the constraint on the particle flow into it, namely

$$I^{(\text{N})}_{\text{e-ph}} = 0, \quad I^{(\text{E})}_{\text{e-ph}} \neq 0. \tag{3.7}$$

  Again, these conditions mirror the particle conservation and the energy loss happening in the carrier-phonon scattering.

- *Recombination reservoir* ($\alpha = \text{rec}$) accounts for the recombination process, in which an electron-hole pair is annihilated and a photon is produced. Unlike the injection reservoir, which describes the creation of carriers from high-energy photons, namely photons of a high-temperature bath, the recombination probe accounts for the carrier interaction with the low-energy photons of the bath at the environment temperature. Indeed, opposite to the injection reservoir, the recombination reservoir depletes both the total number of carriers and the total carrier energy, thereby reducing the resources available to the device. Therefore, this reservoir is

characterized by a thermal distribution at the environment temperature, which coincides with the collector temperature, $T_{\mathrm{rec}} = T_{\mathrm{col}}$, and zero chemical potential, $\mu_{\mathrm{rec}} = 0$, which corresponds to the distribution of carriers at equilibrium with the low-temperature photon bath.

The terminals considered are connected by a single-channel scatterer with transmission probabilities $D_{\alpha,\beta}(E)$. These transmission probabilities account for the strength of the various mechanisms described by the model, as well as the presence of energy filters. Further details can be found in the appended paper [III]. Additionally, we consider electron-hole symmetric systems, as the one depicted in Fig. 3.4, such that the electron and hole transport are completely equivalent and we can focus only on the electronic one. In this symmetric picture, we set the energy lying at the middle of the absorber bandgap to be the zero-energy reference, such that all chemical potentials μ_α are measured starting from there. The electron-hole symmetry allows us to treat transport through the whole device while focusing only on the electron transport, simplifying the discussion of the model. However, many systems are not electron-hole symmetric, see for instance Fig. 3.5. In such a case it is necessary to perform an analogous analysis of the hole transport, and combine it with the electron transport to obtain the whole description of the device. This analysis can again be done using the multi-probe model introduced in paper [III].

3.3.2 Performance quantifiers

Similarly to the thermoelectric heat engine, in paper [III] we characterize the performance of the device through the power output and the efficiency. To this end, we employ the scattering formalism to calculate the currents flowing in the system, namely charge and energy current, which are given by Eqs. (2.10) and (2.11), respectively. However, since we are now focusing only on the electronic transport and the available states in the absorber start from the bottom of the conduction band, which is located at the energy $E_G/2$, the integrals are defined starting from such energy.

Similar to the heat engine, the power produced by the hot-carrier solar cell in the electronic transport is then given by the current extracted by the electronic collector multiplied by its chemical potential, namely

$$P \equiv \mu_{\mathrm{col}} I^{(\mathrm{N})}_{\mathrm{col}}. \tag{3.8}$$

Notice that since we are considering the electron-hole symmetric case and we fixed the zero-energy reference of the system, μ_{col} corresponds to the difference between the collector chemical potential and the Fermi energy of the unbiased device. The power generated by the combined electron and hole transport is simply $2P$.

This power is generated by the combination of multiple terminals. In particular, while the sun reservoir provides all the resources to the device, the electron-electron and electron-phonon probes can also be used in the power production. In the latter chemical potentials are established, meaning that not

only heat is used in the power production. Additionally, the combination of multiple terminals can generate a nonequilibrium distribution of carriers. For these reasons, we do not use the standard heat engine efficiency of Eq. (3.3), but instead we use the nonequilibrium free-energy efficiency to characterize the device. This efficiency is defined as

$$\eta_{\text{global}}^{\text{free}} \equiv \frac{P}{-\sum_{\alpha\neq\text{col}} \dot{F}_{\alpha;\text{col}}} \leq 1, \tag{3.9}$$

where at the denominator lies the sum of the nonequilibrium free-energy currents used in the power production. In particular, the nonequilibrium free-energy is defined as

$$F_{\alpha;\text{env}} \equiv U_\alpha - T_{\text{env}} S_\alpha, \tag{3.10}$$

where T_{env} is the environment temperature, which in our case corresponds to T_{col}. This thermodynamic quantity represents the maximum amount of work that can be extracted from a general nonequilibrium resource when it is put in contact with a thermal bath at the temperature T_{env}, as detailed in App. B. Then, it is clear that the efficiency of Eq. (3.9) is always smaller than 1 due to the second law of thermodynamics. In particular, since all the terminals considered are characterized by a thermal distribution the nonequilibrium free-energy current flowing into terminal α can be decomposed into two terms, namely

$$\begin{aligned}\dot{F}_{\alpha;\text{col}} &= \int_{E_G/2}^{+\infty} \frac{dE}{h} \left[E - \frac{T_{\text{col}}}{T_\alpha}(E-\mu_\alpha)\right] \sum_\beta D_{\alpha,\beta}(E)[f_\beta(E) - f_\alpha(E)] \\ &\equiv \sum_\beta \dot{F}_{\alpha\beta;\text{col}} = \eta_{\text{col},\alpha}^{\text{Carnot}} J_\alpha + \mu_\alpha I_\alpha^{(\text{N})},\end{aligned} \tag{3.11}$$

where $\eta_{\alpha\beta}^{\text{Carnot}} = 1 - T_\alpha/T_\beta$ is the Carnot efficiency between the temperatures of the terminals. The first term corresponds to the maximum heat resource that can be converted into power, namely the heat current multiplied by the Carnot efficiency. Instead, the second term corresponds to the maximum chemical energy that can be converted to power and coincides with the product between the particle current and the chemical energy carried by such particles, the chemical potential μ_α. Unlike the power, the efficiency remains the same when considering both electron and hole transport because both power and nonequilibrium free-energy double.

Imposing the conditions and assumptions made on the terminals, which were discussed previously, one finds that the nonequilibrium free-energy efficiency reduces to

$$\eta_{\text{global}}^{\text{free}} = \frac{P}{-\eta_{\text{col,in}}^{\text{Carnot}} J_{\text{sun}}} \tag{3.12}$$

which corresponds to the heat engine efficiency normalized by the Carnot efficiency. Indeed, the e-e and e-ph probes do not add resources into the system, but only transform the initial heat resource provided by the injection reservoir into a combination of heat and chemical or pure chemical resource,

respectively. Instead, the recombination reservoir only depletes resources in the system. Therefore, the only source of resources is the sun reservoir, and everything that happens between the carrier injection and their extraction to the collector can be understood as the manipulations of a heat engine that allows for dissipation. For this reason the efficiency of Eq. (**??**) is a *global efficiency*, namely an efficiency for the whole device that accounts for the all the losses happening in it.

However, in many setups it is possible to act against only some of such loss mechanisms, or even what are considered to be losses for the power production may be used to perform other useful tasks [104], going against the idea of "loss". Consequently, it is useful to define a *partial efficiency* accounting exclusively for the losses happening in a specific process. Hence, we introduce a partial efficiency accounting only for the losses that happen during the final step of power production, namely the carrier extraction. We define this efficiency as

$$\eta_{\text{neq}}^{\text{free}} \equiv \frac{P}{-\sum_{\alpha\neq\text{col}} \dot{F}_{\alpha,\text{col};\text{col}}} \leq 1, \tag{3.13}$$

which contains, at the denominator, only the components of the nonequilibrium free-energy currents, see Eq. (3.11), that directly contribute to the power production. This novel performance quantifier was used in paper [III] to compare the hot-carrier solar cell in different regimes. The application of the model and the use of these performance quantifiers discussed will be presented in Chapter 5.

Chapter 4

Noise in mesoscopic conductors

This chapter discusses the core topic of papers [I] and [II], namely out-of-equilibrium noise. In particular, we discuss the separation of noise into two contributions: the shot and the thermal contributions. We focus on systems described with the scattering formalism, discussed in Chapter 2, concentrating on two-terminal setups in which both a temperature and a voltage bias are present, as in the thermoelectric devices discussed in Chapter 3. Additionally, we discuss systems in which there are also spin imbalances, and study the spin current fluctuations in such systems. Shot and thermal noise in the presence of voltage and temperature biases, as well as spin imbalances are investigated in papers [I] and [II], which consider a particular case of out-of-equilibrium noise, called delta-T noise, and generalize it to the broader concept of noise in absence of current.

4.1 Shot and thermal noise

Noise is usually considered detrimental because it hinders the accuracy of measurements and the reliability of the device. Indeed, noise does not provide additional information when the system considered is close to equilibrium, where the fluctuation-dissipation theorem holds. To illustrate this, we consider a famous instance of the this theorem: the Johnson-Nyquist noise, which is given by

$$S^I_{\mathrm{th}} = 4Gk_{\mathrm{B}}T. \tag{4.1}$$

Here, G is the electrical conductance defined in Eq. (3.4) and T is the temperature of the system. This noise has its roots in the thermal fluctuations that affect the system, as hinted by the temperature on the right-hand side of Eq. (4.1). Hence, we refer to noise generated by such kind of fluctuations as *thermal noise*. The relation in Eq. (4.1) means that the Johnson-Nyquist noise does not provide additional information on the system. Indeed, one

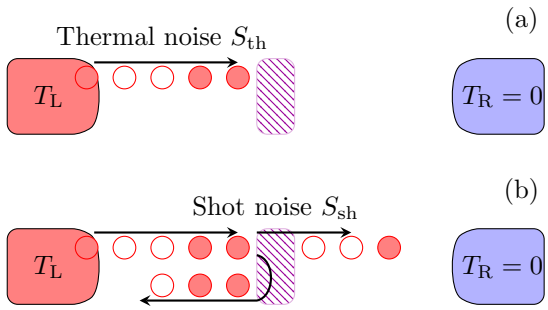

Figure 4.1: Illustration of noise components in a two-terminal system where the left reservoir has finite temperature T_{L}, whereas the right reservoir is at zero temperature, $T_{\text{R}} = 0$. **(a)**: Thermal noise, which is generated by the randomness in the thermal excitations of the electrons. **(b)**: Shot noise, which is generated by the randomness in the current partitioning at the scatterer.

could simply measure the conductance G and the temperature T of the system directly, without measuring the current fluctuations.

However, this relation between fluctuations and dissipation only holds close to equilibrium. In fact, when systems are out of equilibrium, the thermal noise is generally modified and additional noise is observed on top of the thermal noise. This noise is called *shot noise*, or partition noise, and has its origin in the discreteness of the particle transported, in this case electrons. In particular, the name partition is due to the separation of particles at an interface, for instance a scatterer, placed along the direction of the current. This separation introduces additional randomness in the current fluctuations because particles not only may or may not be thermally excited, but also may or may not be transmitted through the scatterer, as illustrated in Fig. 4.1. Hence, shot noise not only requires the system to be out of equilibrium, but also contains additional information on the current statistics. In fact, shot noise has seen many applications, ranging from the characterization of mesoscopic devices [21] to the observation of fractional charges in the quantum Hall effect [22, 23].

Using the framework of scattering theory, as described in Chapter 2, we can calculate the noise in a two-terminal device operating under arbitrary voltage and temperature biases. Clearly, when calculating (or measuring) the noise, both thermal and shot components contribute to the result. Therefore, the separation of the total noise into these two contributions is done according to physical principles. First of all, we define the shot noise as the additional contribution that appear when the system is out of equilibrium. Therefore, the shot noise component must vanish at equilibrium. Additionally, the thermal noise depends crucially on the statistics of the particles emitted by a terminal. In fact, if we consider the electrons emitted at a fixed energy from a terminal such that on average the occupation number is $\langle n \rangle = f$, we can write the fluctuations in the number of electrons as

$$\langle (n - \langle n \rangle)^2 \rangle = \langle n^2 \rangle - \langle n \rangle^2 = \langle n \rangle - \langle n \rangle^2 = f(1 - f). \tag{4.2}$$

To obtain this we used the fermionic nature of electrons, which yields $\langle n \rangle = \langle n^2 \rangle$ due to the Fermi statistics. When the terminal is a reservoir at thermal equilibrium, f takes the form of the Fermi distribution, see Eq. (1.1). Additionally, as one would expect, these fluctuations vanish when the reservoir's temperature approaches zero. Therefore, fluctuations of the kind $f(1-f)$ are typical of thermal noise.

By contrast, shot noise crucially depends on the statistics of the particles transmitted (or reflected) by the scatterer. Consider, for example, the case in which a terminal emits electrons at a given energy with average occupation number $\langle n_{\rm in} \rangle = 1$, namely electrons are always emitted. Then, these electrons impinge on a scatterer and are either transmitted or reflected, with average occupations $\langle n_{\rm T} \rangle = D$ and $\langle n_{\rm R} \rangle = 1 - D$, respectively. Importantly, the correlation between transmitted and reflected electrons is zero, namely $\langle n_{\rm T} n_{\rm R} \rangle = 0$, because after the scattering one between $n_{\rm T}$ and $n_{\rm R}$ is always zero. Indeed, each electron is either transmitted ($n_{\rm T} = 1$, $n_{\rm R} = 0$) or reflected ($n_{\rm T} = 0$, $n_{\rm R} = 1$). This allows us to calculate the fluctuations in the occupation number of transmitted and reflected electrons, which read

$$\langle n_{\rm T}^2 \rangle - \langle n_{\rm T} \rangle^2 = \langle n_{\rm R}^2 \rangle - \langle n_{\rm R} \rangle^2 = D(1-D). \tag{4.3}$$

Interestingly, the fluctuations induced by the randomness of the scattering event have the same structure to the thermal one, namely $x(1-x)$ with x a probability. However, instead of having the occupation probability f, the partition fluctuations are determined by the transmission probability D.

Combining these considerations, we separate the noise obtained with the scattering formalism into a thermal and a shot noise contribution. In particular, for a two-terminal spin-degenerate system, the zero-frequency charge noise is separated into thermal $S^I_{\rm th}$ and shot $S^I_{\rm sh}$ contributions as follows

$$S^I_{\rm th}(0) = \frac{4q^2}{h} \int dE D(E) \sum_{\alpha={\rm L,\ R}} f_\alpha(E)[1 - f_\alpha(E)], \tag{4.4}$$

$$S^I_{\rm sh}(0) = \frac{4q^2}{h} \int dE D(E)[1 - D(E)][f_{\rm L}(E) - f_{\rm R}(E)]^2. \tag{4.5}$$

As wanted, the thermal contribution in Eq. (4.4) contains the thermal fluctuations $f(1-f)$ of both terminals and is finite at equilibrium. By contrast, the shot contribution in Eq. (4.5) contains the partition fluctuations $D(1-D)$ of the scatterer and vanishes at equilibrium, namely when $f_{\rm L}(E) = f_{\rm R}(E)$ for all energies.

While Eqs. (4.4) and (4.5) are the thermal and shot contribution to the charge current noise, this separation of the noise can be applied also to other quantities, for instance heat and spin currents, as discussed in the following.

4.2 Heat and spin noise

Charge noise is the noise studied the most both theoretically and experimentally because of its accessibility. Indeed, accurate measurements of charge currents

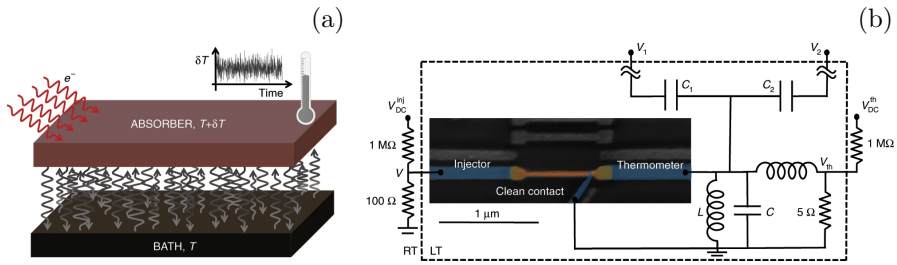

Figure 4.2: **(a)**: The thermometer measures the absorber temperature $T + \delta T$, which is affected by the fluctuations of the heat exchanged with the bath or injection of hot-electrons. **(b)**: Measurement setup including scanning electron micrograph. The absorber (brown) is connected to two superconducting leads (blue) acting as thermometer and injector. **Source**: [109].

can be achieved in particular in mesoscopic systems thanks to current amplifiers. Nevertheless, access to fluctuations of other kinds of quantities can provide further insights into the system investigated. In particular, here we consider the fluctuations of heat currents and spin currents.

Heat current fluctuations reveal features that are not shown in charge noise [105], and can be used as a tool to detect coherence and entanglement in open quantum systems [106]. Additionally, they are crucial in the fields of stochastic and quantum thermodynamics, where fluctuations allow to probabilistically violate the second law of thermodynamics, while fulfilling it on average. However, measuring heat currents in quantum systems is challenging because they are small in magnitude (ranging between 0.1 and 100 pW at cryogenic temperatures) [107]. Nonetheless, indirect measurements of heat flows have been performed by complete electrical characterization of the system. For example, this can be done by detecting single electron transitions across a junction in a single-electron box [108]. Recently, a direct measurement of temperature fluctuations was performed at sub-Kelvin temperatures [109], in the setup illustrated in Fig. 4.2. These temperature fluctuations are directly generated by the fluctuations of the heat current between the substrate thermal bath and the sample observed (namely the absorber in Fig. 4.2). Therefore, the possibility of accessing heat fluctuations allows further investigation of out-of-equilibrium and quantum thermodynamics [107, 110].

Similarly, spin currents are difficult to measure, but the fluctuations associated with them can provide useful insights into the system. In particular, the presence of spin currents modifies the charge current noise, which can instead be easily detected. Such modifications can be used to measure the spin injection efficiency from a ferromagnet [111], or to reveal information on the relative orientation between ferromagnets [112] and the spin relaxation processes [113]. Additionally, the charge current noise allows to detect spin accumulations [114]. This last application was recently proven experimentally [115], albeit without exploring the regime in which only a pure spin current flows in the system, namely when the charge current vanishes. Clearly, spin

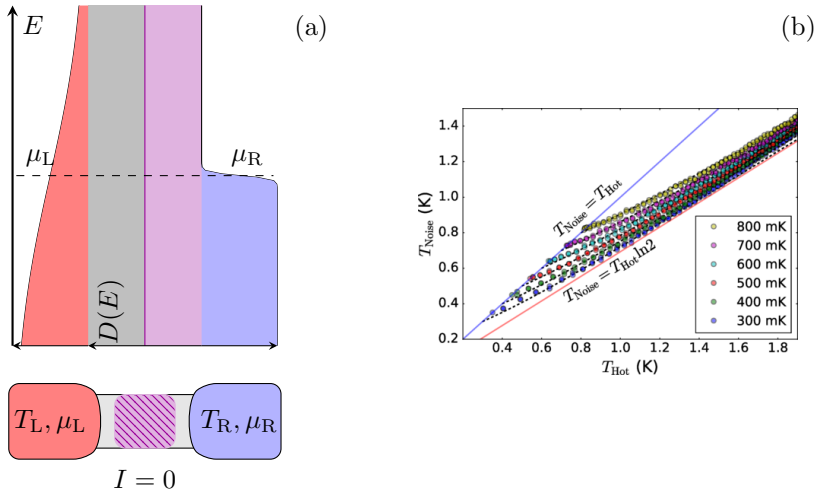

Figure 4.3: **(a)**: Schematic setup used to measure the delta-T noise in electron-hole symmetric systems. The transmission probability $D(E) = D$ is uniform, so the temperature bias alone does not induce a charge current. The two terminals are kept at the same chemical potential, $\mu_L = \mu_R$ but have different temperatures. **(b)**: Experimental data of noise equivalent temperature T_{Noise} at different contact temperatures, T_{Hot} (x-axis) and T_{Cold} (legend). Out of equilibrium, i.e. when T_{Hot} is not close to T_{Cold}, the noise deviates from the Johnson-Nyquist noise (blue) and instead approaches $T_{Hot} \ln 2$ (red). **Source**:[57]

currents are crucial in the field of spintronics, and the information revealed by fluctuations in spintronic devices can further boost the research in that field.

4.3 Delta-T and zero-current noise

The studies done in papers [I] and [II] stem from the notion of *delta-T* noise. This noise was recently measured for the first time in Ref. [24], and since then other experiments [56, 57, 107, 116, 117] and theoretical studies [118–122] have been performed. This kind of noise emerges when only a temperature bias is imposed on the system, hence the name delta-T noise. In particular, these first measurements have been performed in electron-hole symmetric systems, in which a pure temperature bias does not induce any charge current. Therefore, the delta-T noise is an instance of noise in absence of currents.

Spefically, the setups of many of such experiments can be schematically pictured as in Fig. 4.3 (a), where a scatterer with uniform transmission probability $D(E) = D$ makes the system electron-hole symmetric. Therefore, a pure temperature bias does not generate any charge current. In fact, the charge current carried by electrons flowing above the Fermi energy is balanced by the one carried by the holes flowing below it. In such a setup the thermal noise

contribution of Eq. (4.4) becomes

$$S^I_{\rm th} = \frac{4e^2}{h} D k_{\rm B} \left[T_{\rm L} + T_{\rm R}\right], \tag{4.6}$$

which is proportional to the sum of the contact temperatures. Additionally, if the hot temperature is much larger than the cold one, we can approximate the latter as the zero temperature. Here, we take without loss of generality the right contact to be the colder one. The low temperature assumption simplifies the calculations and allows us to approximate the shot noise contribution of Eq. (4.5) as [21]

$$S^I_{\rm sh} \approx \frac{4e^2}{h} D(1-D) k_{\rm B} T_{\rm L} \left[2\ln 2 - 1\right]. \tag{4.7}$$

In particular, if the scatterer is very opaque, namely the transmission probability is small $D \ll 1$, the total noise contribution becomes

$$S^I \approx \frac{8e^2}{h} D k_{\rm B} T_{\rm L} \ln 2. \tag{4.8}$$

This result was shown experimentally in Ref. [57], the data of which is shown in Fig. 4.3, where the noise is quantified in terms of the noise equivalent temperature $T_{\rm Noise}$. This temperature corresponds to the temperature that both contacts need to be at for achieving the same amount of equilibrium noise, namely

$$S^I = \frac{8e^2}{h} D k_{\rm B} T_{\rm Noise}. \tag{4.9}$$

Here, the transition between the near equilibrium regime and the out-of-equilibrium regime is apparent: When the contact temperatures are close to each other the fluctuation-dissipation theorem holds, and the noise equivalent temperature coincides with the hot temperature. Instead, when the contact temperatures differ greatly the noise equivalent temperature becomes $T_{\rm Hot} \ln 2$, see Eq. (4.8). This additional noise is provided by the shot noise contribution. Importantly, for the shot noise to emerge it is not required that a finite charge current is present, but that the system is subject to an out-of-equilibrium condition.

Papers [I] and [II] enlarge the scope of inquiry around the delta-T noise by considering the more general noise in absence of currents. Indeed, the noise in absence of currents allows us to consider systems that are not electron-hole symmetric. In such systems the zero-current condition is generally achieved by having both a temperature and a voltage bias. This allows us to study the impact that the out-of-equilibrium condition has on the fluctuations in more generic systems. In fact, this noise also allows us to generalize the delta-T noise to other kinds of currents, like the heat and the spin currents described in Sec. 4.2. Having a vanishing average current is also favourable for comparing the out-of-equilibrium noise with the fluctuation-dissipation theorem. In fact, the latter holds at equilibrium, where the average currents vanish. Additionally, the zero-current condition was shown to yield an out-of-equilibrium extension

of the fluctuation-dissipation theorem for systems obeying the local detailed balance principle [58]. Therefore, investigating this kind of noise provides a better understanding of fluctuations in systems out of equilibrium.

Chapter 5

Results

In the previous chapters we provided an introduction to the general scientific context, as well as more detailed information about the formalism and the setups considered in the appended papers. Additionally, the model proposed in paper [III] was described in Sec. 3.3. Therefore, the previous chapters provide the basic background to understand the contents and the results of the appended papers. This chapter gathers the main findings.

5.1 Shot noise in absence of currents

As discussed in Sec. 4.1, to have a finite shot noise it is necessary for the system to be out of equilibrium. Importantly, this condition can still be achieved when the average current vanishes. The shot noise in absence of currents is studied in papers [I,II], and their results are discussed jointly in this section. In particular, paper [I] focuses on the zero-frequency noise in charge and heat transport. Paper [II] expands the studies on noise in absence of currents by considering also spin currents, finite-frequency noise, and by improving the results of paper [I]. These papers show that the heat shot noise can be arbitrarily large even in the absence of an average heat current. In particular, we prove that the heat fluctuations can be dominated by the shot noise. Additionally, in spin-nondegenerate systems it is possible to achieve the zero-current condition for charge and spin transport without any temperature bias. Therefore, when the voltage bias or spin imbalance is much larger than the system temperature, the thermal noise becomes neglible, and only the shot noise contributes the fluctuations. Finally, in spin-degenerate systems, in which charge transport is controlled through voltage and temperature biases, we prove that the zero-current charge shot noise is *always* limited by its thermal counterpart. This bound also holds on the finite-frequency shot noise, and limits the influence of shot noise on the zero-current charge fluctuations generated using a temperature bias.

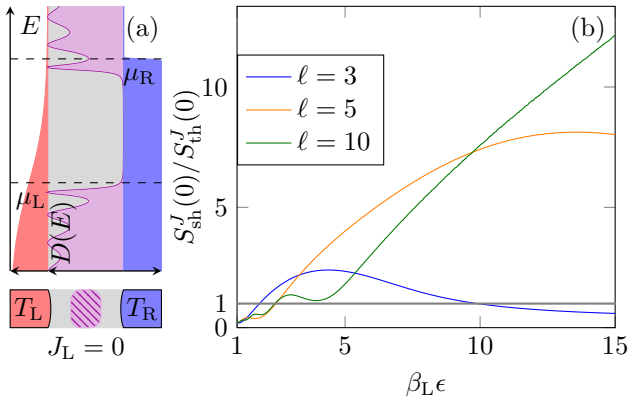

Figure 5.1: **(a)**: Zero heat current condition achieved for the transmission probability $D(E)$ depicted. **(b)**: Ratio between zero-frequency heat shot noise and heat thermal noise when varying the parameters of the transmission. The shot noise can be much larger than the thermal noise.

5.1.1 Heat current noise

We consider a spin-degenerate setup similar to those described in Chapter 3, illustrated in Fig. 5.1(a), where only a temperature and a chemical potential bias are present. In paper [I] we show that, for a Lorentzian transmission, the heat shot noise is smaller than the heat thermal noise. However, this is not the case for all types of conductors. In fact, in the same paper, it is also demonstrated that, with an appropriate transmission, the shot noise can be arbitrarily large while the thermal noise remains finite. The transmission used in paper [I] to show this is rather mathematical, and does not have a direct physical counterpart. Nonetheless, it illustrates the main features necessary to obtain large heat shot noise, namely that the transmission should have two transmission windows which are distant in energy. Paper [II] uses this insight to show that the heat shot noise can become much larger than the thermal noise in an experimentally feasible transmission, depicted in Fig. 5.1 (see appended paper [II] for details). This transmission was shown in Ref. [123] to be the two-terminal transmission for a quantum spin Hall edge [124] coupled to a small magnetic island with characteristic length and energy scales ℓ and $\epsilon_\perp$, respectively. This setup allows to obtain heat shot noise much larger than the thermal noise, as illustrated in Fig. 5.1(b). Therefore, even in the absence of an average heat flow, it is possible to achieve large heat shot noise. The fundamental reason why this happens is that heat grows with the energy of the transferred particle. In particular, while the heat current contains the heat $(E - \mu_L)$, the noise contains $(E - \mu_L)^2$, which grows faster at large energies, and thereby leads to larger contributions when the transmission windows are distant in energy.

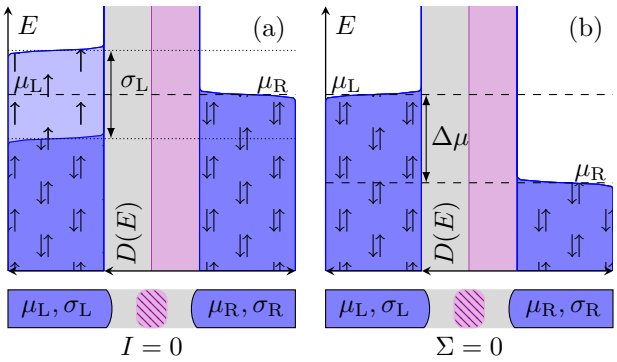

Figure 5.2: **(a)**: Zero charge current condition achieved with the spin imbalance σ_L between the spin populations of the left contact. **(b)**: Zero spin current condition achieved without any spin imbalances, but with the chemical potential difference $\Delta\mu$ between the contacts.

5.1.2 Spin current noise

On the other hand, when considering spin currents, we consider spin-nondegenerate systems. In particular, we allow the spin populations in each terminal to be characterized by different distributions, that we indicate with $f_{\alpha\tau}(E)$, where $\alpha = \mathrm{L}, \mathrm{R}$ indicates the contact, while $\tau = \uparrow, \downarrow$ indicates the spin. Electrons with different spin in the same contact may have different chemical potentials [115]. We refer to this difference as spin imbalance. Spin transport is mediated by electrons from the contacts undergoing scattering processes, which we assume to be spin-conserving, such that the spins of an electron before and after the scattering event coincide. Then, we calculate the zero-frequency noise of the spin current generated in such a way, and serapate it into its thermal and shot components, obtaining

$$S^{\Sigma}_{\mathrm{th}}(0) = \sum_{\tau} \frac{2}{h} \int dE \left(\frac{(-1)^{\delta_{\tau\uparrow}} \hbar}{2} \right)^2 D_{\tau}(E) \sum_{\alpha=\mathrm{L},\mathrm{R}} f_{\alpha\tau}(E)[1 - f_{\alpha\tau}(E)], \quad (5.1)$$

for the thermal noise, and

$$S^{\Sigma}_{\mathrm{sh}}(0) = \sum_{\tau} \frac{2}{h} \int dE \left(\frac{(-1)^{\delta_{\tau\uparrow}} \hbar}{2} \right)^2 D_{\tau}(E)[f_{\mathrm{L}\tau}(E) - f_{\mathrm{R}\tau}(E)]^2, \quad (5.2)$$

for the shot noise. Here, the quantity in the round brackets is the spin carried by the electrons, while $D_{\tau}(E)$ is a spin-dependent transmission probability preserving the particle spin.

Having different spin populations increases the control parameters of the system, and makes it similar to a spinless four-terminal setup. These additional control parameters allow to reach large shot noise in the absence of currents. In particular, we consider now the case in which the contact temperatures are equal and much smaller than the voltage bias between the contacts or the spin

imbalances, such that we can approximate them with the zero temperature. This means that the thermal noise contribution to the fluctuations are negligible compared to the shot noise contributions. Additionally, we consider a uniform and spin-independent transmission probability, namely $D_\tau(E) = D$. Under these conditions, we study the noise in absence of currents. First, we consider the case in which there is no voltage bias between the contacts, but the left contact has a finite spin imbalance σ_{L}, such that the spin populations distributions are

$$f_{\mathrm{L}\tau}(E) = f_{\mathrm{L}}(E + (-1)^{\delta_{\tau\uparrow}}\sigma_{\mathrm{L}}/2). \tag{5.3}$$

Instead, the right contact as no spin imbalance. This configuration is illustrated in Fig. 5.2, and has no average charge current. Indeed, the charge current carried by the spin-↑ electrons flowing above the Fermi energy is balanced by the one carried by the spin-↓ electrons flowing below the Fermi energy. Nonetheless, the total charge current noise is finite, and uniquely given by the shot noise contribution, namely

$$S^I(0) = \frac{2e^2}{h} D(1-D)\sigma_{\mathrm{L}}. \tag{5.4}$$

Notably, the charge current noise is directly proportional to the spin imbalance σ_{L}. Therefore, by measuring the charge current fluctuations in the absence of average charge current it is possible to detect the presence of spin imbalances.

Instead, by considering the case in which there is no spin imbalance in either contact, but there is a voltage bias between them inducing the chemical potential difference $\Delta\mu = \mu_{\mathrm{L}} - \mu_{\mathrm{R}}$, we reach an out-of-equilibrium setup in which the average spin current vanishes. This setup is illustrated in Fig. 5.2(b), and has clearly no net spin current because the contribution of the spin-↑ electrons balances with the contribution of the spin-↓ electrons. Nonetheless, the total spin current noise is finite, and reads

$$S^\Sigma(0) = \frac{\hbar}{2\pi} D(1-D)\Delta\mu, \tag{5.5}$$

which again coincides with the shot noise since the temperatures are low. Similarly to the charge fluctuations in Eq. (5.4), also the spin fluctuations in Eq. (5.5) are directly proportional to the bias imposed on the system, in this case the voltage bias $\Delta\mu/(-e)$.

5.1.3 Charge current noise

We now consider the charge current fluctuations when the average charge current vanishes. In particular, we study two-terminal, spin-degenerate setups in which both a temperature and a voltage bias are present, as the thermoelectric devices described in Chapter 3.

Unlike the previous cases of Secs. 5.1.1 and 5.1.2, here the shot noise behaves differently. In particular, in paper [I] we show that the charge shot noise is always smaller than the thermal noise. We further improved upon this bound

in paper [II], resulting in the following inequality chain on the zero-frequency noise components:

$$S^I_{\rm sh}(0) \leq \Theta_{\rm h} - \Theta_{\rm c} \leq \Theta_{\rm h} + \Theta_{\rm c} = S^I_{\rm th}(0) \tag{5.6}$$

where

$$\Theta_{\rm h/c} = \frac{4e^2}{h}\int dE D(E) f_{\rm h/c}(E)[1 - f_{\rm h/c}(E)] \tag{5.7}$$

is the contribution to the thermal noise of the hot (h) or cold (c) contact. Crucially, the bound in Eq. (5.6) holds for *any transmission probability* $D(E)$ and *any temperatures* $T_{\rm L}$, $T_{\rm R}$, as long as the chemical potential difference is chosen to satisfy the zero-current condition. Therefore, this bound between shot and thermal noise is both general and fundamental. Interestingly, the first inequality in Eq. (5.6), which was proven in paper [II], correctly recovers the behavior of shot noise close to equilibrium. Indeed, when the temperatures of the contacts are close together, their thermal noise contributions are similar, namely $\Theta_{\rm h} - \Theta_{\rm c} \approx 0$, making the shot noise vanishingly small compared to the thermal noise.

Furthermore, in paper [II] we proved that even at finite frequency the shot noise is bounded by the remaining noise contributions, which include the thermal noise, albeit with a less strict bound and with an additional condition. In fact, measuring the noise without loss of generality on the left contact, the finite-frequency shot noise is limited by

$$S^I_{\rm sh}(\omega) \leq S^I_{\rm rest}(\omega) - \mathcal{R}(\omega) - \Theta_{\rm L}(\omega) \leq S^I_{\rm rest}(\omega), \tag{5.8}$$

as long as the current fluctuations are *measured in the cold contact*, namely $T_{\rm L} \leq T_{\rm R}$. The terms introduced in Eq. (5.8) are both frequency-dependent and positive, see appended paper [II] for the details. Similarly to the zero-frequency bound, the finite-frequency bound in Eq. (5.8) holds for *any transmission probability* $D(E)$ and *any temperatures satisfying* $T_{\rm L} \leq T_{\rm R}$, as long as the chemical potential difference is chosen to satisfy the zero-current condition. The requirement of measuring the noise on the cold contact is due to the fact that, at finite-frequency, the current correlators do not satisfy the noise power conservation rules that stem from particle conservation [66], and noise depends on where it is measured.

Interestingly, it is possible to overcome the first inequality in Eq. (5.8) when the noise is measured in the hot contact. Nonetheless, a numerical analysis did not show any instance of finite-frequency shot noise being larger than the remaining fluctuations even if the measurement is carried on the hot contact. Therefore, we conjecture the charge shot noise to be always bounded under the zero-current condition, for any transmission probability $D(E)$, temperatures $T_{\rm L}$, $T_{\rm R}$, and frequency ω.

5.2 Quantum transport in a hot-carrier solar cell

In paper [III] we introduce the novel transport model and performance quantifiers, discussed in Sec. 3.3, to describe a hot-carrier solar cell. In particular, we use Büttiker probes to mimic the effects of carrier-carrier and carrier-phonon scattering, which lead to carrier thermalization and relaxation to the lattice temperature, respectively. Additionally, we study the performance of the device by considering, in addition to the power, a global and a partial efficiency, both of which are based on the nonequilibrium free energy. By changing the balance between the different loss mechanisms, the multi-probe model ranges among different regimes, from the solar engine, in which there are no such losses, to the conventional solar cell, in which all the carrier excess energy is lost to the lattice. Between such regimes lie the cell exploiting thermalized hot-carriers, in which the carriers take on a thermal distribution at a temperature higher than the lattice, and the cell exploiting nonequilibrium hot-carriers, in which the carriers take on a nonequiliubrium distribution. Interestingly, extracting a nonequilibrium carrier distribution improves the performance of the device.

Nonetheless, if the carrier thermalization is fast, their distribution is thermal. In this case, in paper [III] we prove that a boxcar-shaped transmission maximizes the efficiency at any given power output, thereby extending the result of Refs. [88, 89] to systems in which both a temperature and a chemical potential bias are used to generate power.

5.2.1 Regimes in the multi-probe model

The different contacts making up the multi-probe model are described in Sec. 3.3.1. Transport between these terminals is mediated by a scatterer connecting them with transmission probabilities $D_{\alpha,\beta}(E)$ of tunneling from contact β to contact α. These transmissions regulate how often the corresponding process happens. In particular, by choosing the transmission probabilities appropriately, we can explore different regimes in which the device operates. The regimes considered are illustrated in Fig. 5.3, and are briefly explained below (more details are found in appended paper [III]).

(a) The *ideal solar engine* is obtained when no loss mechanism happens. Then, the carriers take on the a thermal distribution at the sun's temperature and the device operates as a thermoelectric heat engine.

(b) The *cell exploiting thermalized hot-carriers* is obtained when the carriers are extracted after they thermalize between themselves through electron-electron interaction, but before they lose all their excess energy to the lattice through electron-phonon interaction. In this case the carriers establish well-defined temperature higher than the lattice temperature and a finite chemical potential, both of which are used to produce power.

(c) The *conventional solar cell* is obtained when the carriers relax to the lattice temperature through electron-phonon interaction before being

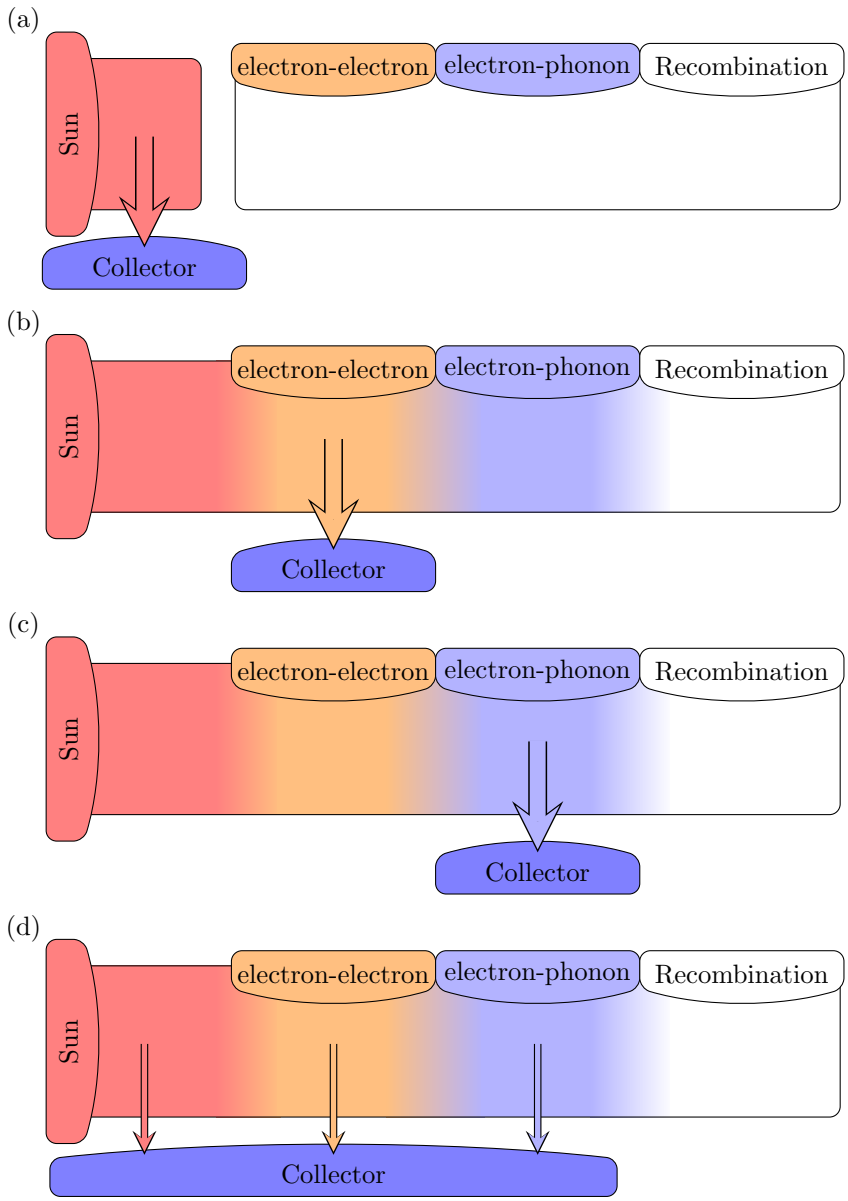

Figure 5.3: Schematic representation of the regimes of operation considered. **(a)**: Ideal solar engine in which there are no loss mechanisms. **(b)**: Thermalized hot-carrier solar cell, in which the extracted carriers have thermalized and reached a well defined temperature $T_{\text{e-e}}$ and chemical potential $\mu_{\text{e-e}}$. **(c)**: Solar cell, in which the extracted carriers have relaxed to the lattice temperature T_{col}, while having chemical potential $\mu_{\text{e-ph}}$. **(d)**: Nonequilibrium hot-carrier solar cell, in which the extracted carriers are described by a nonthermal distribution, in this case a combination of the former.

extracted. In this case all the excess energy of the carriers is lost, and the carriers take on the ambient temperature, but establish a finite chemical potential, which is used to produce power.

(d) The *cell exploiting nonequilibrium hot-carriers* is obtained when the device exploits the nonequilibrium nature of the hot carriers. To obtain the nonequilibrium carrier distribution, all kinds of carriers are extracted equally. In this case the carriers extracted by the collector do not exhibit a well-defined temperature or chemical potential.

Unsurprisingly, the ideal solar engine produces more power and does so with a better global efficiency compared to the other regimes. In fact, the ideal solar engine does not have any loss mechanism. On the opposite, the conventional solar cell has the lowest power output and global efficiency of the regimes considered because it incurs in more losses. By contrast, the picture is reversed for the partial efficiency. In fact, since the solar cell exploits cold carriers to produce power, it extracts them more efficiently compared to the other regimes, in which the carrier distributions are spread in energy. Both the thermalized and nonequilibrium hot-carrier solar cells produce more power with a higher global efficiency than the conventional solar cell because they do not have as many losses. However, the use of a nonequilibrium carrier distribution improves the power generated by the cell while operating at the same global efficiency of the thermalized hot-carrier solar cell.

5.2.2 Best efficiency at a given power

The second major achievement of paper [III] is obtained when the device exploits a thermal distribution, irrespective of the origin of its temperature and chemical potential. Therefore, this covers the ideal solar engine, the thermalized hot-carrier solar cell, and the conventional solar cell discussed previously. For such regimes we prove that the boxcar-shaped transmission, defined as

$$D(E) = \begin{cases} 1 & \text{for } E_0 < E < E_1 \\ 0 & \text{otherwise} \end{cases} , \tag{5.9}$$

maximizes the extraction efficiency at any given power output for an appropriate choice of the initial (E_0) and final (E_1) energy. This kind of transmission was already recognized to be optimal for thermoelectric heat engines in Refs. [88, 89]. Here, we generalize it to systems in which also a chemical potential is present, influencing the choices of E_0 and E_1.

The proof is based on a variational analysis that can be found in paper [III]. Importantly, the proof requires the carrier distribution to be thermal, thereby excluding the nonequilibrium hot-carrier solar cell regime. Nonetheless, we expect a boxcar with a suitable choice of width and position, or possibly a combination of multiple distinct boxcars, to be optimal even for nonthermal distributions.

Chapter 6

Conclusions

6.1 Summary

This thesis studies transport in out-of-equilibrium systems focusing on two different aspects: the current fluctuations under out-of-equilibrium conditions, and the effect of nonequilibrium (or nonthermal) distributions as a resource.

On the one hand, we investigate the current fluctuations in various mesoscopic systems, with particular focus on thermoelectric devices. These fluctuations become particularly interesting out of equilibrium, where the shot noise contribution is finite, even if the average current vanishes. We find that, even with vanishing average current, the heat shot noise can be arbitrarily large. The same applies to both charge and spin shot noise in spin-nondegenerate systems. Instead, in spin-degenerate systems in which the zero-current condition is achieved by means of a temperature and a voltage bias, we prove that the charge shot noise is always smaller than the thermal one.

On the other hand, we analyze a hot-carrier solar cell, where we propose a transport model to describe the main loss mechanisms happening. This particular device combines the thermoelectric and the photovoltaic effects, and its working principle relies on the fast carrier extraction, which can exploit nonthermal carrier distributions. Therefore, we tackle the crucial task to investigate the effects of nonequilibrium distribution on the performance of the device. We find that the extraction of a nonequilibrium carrier distribution indeed improves the power generated by the device. Nonetheless, if the carrier distribution is thermal, we prove that the maximum efficiency at any given power output is obtained using a boxcar-shaped transmission, see Eq. (5.9).

6.2 Outlook

The presented results lay the basis for a number of open questions, which are briefly described in the following.

First, in Sec. 5.1.3 a conjecture is presented, namely that the finite frequency charge shot noise in absence of current is smaller than its thermal counterpart

even when the noise is measured on the hotter contact. Proving this would further reinforce the generality of the bound on charge shot noise in absence of currents. Additionally, the results of paper [I] and [II] raise questions about the existance of an analogous bound in interacting or bosonic systems, which would be interesting to investigate in the future.

Concerning the hot-carrier solar cell analysis, on the other hand, the results of paper [III] beg for an application of the model to realistic systems, like devices based on nanowires heterostructures or 2D graphene sheet, and for a deeper analysis of the nonequilibrium effects on the performance of the device.

These different aspects of out-of-equilibrium thermodynamics could also be combined. In fact, studying the noise generated by nonequilibrium distributions, for which the bound on shot noise is not guaranteed to hold, is interesting. For example, fluctuations could be useful in distinguishing a "pure" nonequilibrium resource, namely a reservoir described by a nonequibrium distribution, from an "artificially" generated nonequilibrium distribution, namely a distribution obtained by the mixing of thermal ones. In particular, the latter is what is considered in paper [III], as well as in Refs. [18, 19], where the nonequilibriumness of a distribution is used to power a refrigerator.

Last, we mention that the bound obtained on shot noise is different from the thermodynamic uncertainty relations. In fact, in our result, only the shot and thermal current noise components appear, whereas in the thermodynamic uncertainty relations the total current noise as well as the entropy production and the average charge current do. Investigating whether a connection between such inequalities exists or how they can be combined can provide further insights into the out-of-equilibrium fluctuations.

Appendix A

Probability current and current operators

The probability density $n(\boldsymbol{x},t)$ of finding a non-relativistic particle around the position $\boldsymbol{x}$ at time t evolves according to

$$\begin{aligned}\partial_t n(\boldsymbol{x},t) &= \partial_t \left|\psi(\boldsymbol{x},t)\right|^2 = [\partial_t\psi^*(\boldsymbol{x},t)]\psi(\boldsymbol{x},t) + \psi^*(\boldsymbol{x},t)\partial_t\psi(\boldsymbol{x},t),\\ &= \frac{i}{2m\hbar}\left[[\hat{\boldsymbol{p}}^2\psi^*(\boldsymbol{x},t)]\psi(\boldsymbol{x},t) - \psi^*(\boldsymbol{x},t)\hat{\boldsymbol{p}}^2\psi(\boldsymbol{x},t)\right],\\ &= \frac{i\hbar}{2m}\boldsymbol{\nabla}\left[\psi^*(\boldsymbol{x},t)\boldsymbol{\nabla}\psi(\boldsymbol{x},t) - [\boldsymbol{\nabla}\psi^*(\boldsymbol{x},t)]\psi(\boldsymbol{x},t)\right],\end{aligned} \tag{A.1}$$

where the Schrödinger equation was used to determine the evolution of the wavefunction $\psi(\boldsymbol{x},t)$. The operator $\hat{\boldsymbol{p}}$ is the momentum operator, which, in the coordinate representation becomes proportional to the spatial derivatives, namely $\hat{\boldsymbol{p}} = -i\hbar\boldsymbol{\nabla}$. The last line of Eq. (A.1) highlights the structure of the probability density evolution, which take the form of a continuity equation, namely

$$\partial_t n(\boldsymbol{x},t) + \boldsymbol{\nabla}\boldsymbol{\mathcal{J}}(\boldsymbol{x},t) = 0. \tag{A.2}$$

Here $\boldsymbol{\mathcal{J}}(\boldsymbol{x},t)$ is the probability current of the particle, and is defined as

$$\boldsymbol{\mathcal{J}}(\boldsymbol{x},t) \equiv -\frac{i\hbar}{2m}\left\{\psi^*(\boldsymbol{x},t)\boldsymbol{\nabla}\psi(\boldsymbol{x},t) - [\boldsymbol{\nabla}\psi^*(\boldsymbol{x},t)]\psi(\boldsymbol{x},t)\right\}. \tag{A.3}$$

Using this quantum-mechanical notion of current we calculate the current operators in the scattering formalism by substituting the particle field $\Psi_\alpha(\boldsymbol{r},t)$ in place of the wavefunction $\psi(\boldsymbol{x},t)$. In particular, the currents flowing across lead α are obtained by integrating the flow in the direction of the lead along the direction perpendicular to the particle propagation, namely $r_\perp$. In particular, using the shorthand notation $\bullet = \bullet(E)$ and $\bullet' = \bullet(E')$, for the charge current

we have

$$\begin{aligned}\hat{I}_\alpha &= -\frac{iq\hbar}{2m}\int dr_\perp \left[\Psi^\dagger_\alpha(\boldsymbol{r},t)\partial_x\Psi_\alpha(\boldsymbol{r},t) - [\partial_x\Psi^\dagger_\alpha(\boldsymbol{r},t)]\Psi_\alpha(\boldsymbol{r},t)\right] \\ &= -\frac{iq\hbar}{2m}\int dr_\perp dE dE' \sum_{ii'} \frac{\chi_{\alpha i}\chi'^*_{\alpha i'}}{\sqrt{hvhv'}} e^{-i(E-E')t/\hbar}\times \\ &\times \left\{-ik\left[\hat{a}'^\dagger_{\alpha i'}e^{ik'x} + \hat{b}'^\dagger_{\alpha i'}e^{-ik'x}\right]\left[\hat{a}_{\alpha i}e^{-ikx} - \hat{b}_{\alpha i}e^{ikx}\right]\right. \\ &\left. -ik'\left[\hat{a}'^\dagger_{\alpha i'}e^{ik'x} - \hat{b}'^\dagger_{\alpha i'}e^{-ik'x}\right]\left[\hat{a}_{\alpha i}e^{-ikx} + \hat{b}_{\alpha i}e^{ikx}\right]\right\}.\end{aligned} \tag{A.4}$$

Now, the approximations done in Sec. 2.2 allow us to greatly simplify the calculations. Indeed, the orthonormality of $\chi_{\alpha i}(E, r_\perp)$ can then be used, yielding a Kronecker delta $\delta_{ii'}$. Additionally, when $k = k'$ the annihilation and creation operators simplify, and since $\hbar k(E) = mv(E)$ the particle velocities disappear. For this cancellation to happen it is crucial that the propagation happens in a one-dimensional lead. In the end, we get the simple formulation in Eq. (2.6).

One can proceed in a similar fashion for the energy and spin currents, placing the operator corresponding to the quantity of interested between $\Psi^\dagger_\alpha(\boldsymbol{r},t)$ (or $\partial_x\Psi^\dagger_\alpha(\boldsymbol{r},t)$) and $\partial_x\Psi_\alpha(\boldsymbol{r},t)$ (or $\Psi_\alpha(\boldsymbol{r},t)$). For example, the energy current is obtained by considering the flow for the Hamiltonian $\hat{H}$, which yields

$$\begin{aligned}\hat{I}^{(\mathrm{E})}_\alpha &= -\frac{i\hbar}{2m}\int dr_\perp \left[\Psi^\dagger_\alpha(\boldsymbol{r},t)\hat{H}\partial_x\Psi_\alpha(\boldsymbol{r},t) - [\partial_x\Psi^\dagger_\alpha(\boldsymbol{r},t)]\hat{H}\Psi_\alpha(\boldsymbol{r},t)\right] \\ &= -\frac{i\hbar}{m}\int dr_\perp dE dE' \left(\frac{E+E'}{2}\right) \sum_{ii'} \frac{\chi_{\alpha i}\chi'^*_{\alpha i'}}{\sqrt{hvhv'}} e^{-i(E-E')t/\hbar}\times \\ &\times \left\{-ik\left[\hat{a}'^\dagger_{\alpha i'}e^{ik'x} + \hat{b}'^\dagger_{\alpha i'}e^{-ik'x}\right]\left[\hat{a}_{\alpha i}e^{-ikx} - \hat{b}_{\alpha i}e^{ikx}\right]\right. \\ &\left. -ik'\left[\hat{a}'^\dagger_{\alpha i'}e^{ik'x} - \hat{b}'^\dagger_{\alpha i'}e^{-ik'x}\right]\left[\hat{a}_{\alpha i}e^{-ikx} + \hat{b}_{\alpha i}e^{ikx}\right]\right\}.\end{aligned} \tag{A.5}$$

Where we used $\hat{H} = \hat{H}^\dagger$ to make the operator act on $\Psi_\alpha(\boldsymbol{r},t)$ and $\Psi^\dagger_\alpha(\boldsymbol{r},t)$ respectively.

As stated in the main text, when we also consider the spin of the particles, we can include the corresponding index τ in the reservoir index. In spin-degenerate systems, this only adds a degeneracy factor (2 for electrons). However, we can also use it to calculate spin transport quantities. In this case, the spin current operator is obtained by considering the flow of the particle spin. For electrons, this corresponds to the operator $\hat{s} = \hbar\hat{\sigma}_z/2$, where $\hat{\sigma}_z$ is the Pauli matrix, and

yields

$$\begin{aligned}\hat{\Sigma}_\alpha &= -\frac{i\hbar}{2m}\int dr_\perp \left[\Psi^\dagger_\alpha(\boldsymbol{r},t)\hat{s}\partial_x\Psi_\alpha(\boldsymbol{r},t) - [\partial_x\Psi^\dagger_\alpha(\boldsymbol{r},t)]\hat{s}\Psi_\alpha(\boldsymbol{r},t)\right] \\ &= -\frac{i\hbar}{m}\int dr_\perp dE dE' \sum_{ii'\tau\tau'} \frac{\hbar}{2}\left(\frac{(-1)^{\delta_{\tau\downarrow}} + (-1)^{\delta_{\tau'\downarrow}}}{2}\right)\frac{\chi_{\alpha\tau i}\chi'^*_{\alpha\tau' i'}}{\sqrt{hvhv'}}\times \\ &\times e^{-i(E-E')t/\hbar}\left\{-ik\left[\hat{a}'^\dagger_{\alpha\tau' i'}e^{ik'x} + \hat{b}'^\dagger_{\alpha\tau' i'}e^{-ik'x}\right]\left[\hat{a}_{\alpha\tau i}e^{-ikx} - \hat{b}_{\alpha\tau i}e^{ikx}\right]\right. \\ &\left. -ik'\left[\hat{a}'^\dagger_{\alpha\tau' i'}e^{ik'x} - \hat{b}'^\dagger_{\alpha\tau' i'}e^{-ik'x}\right]\left[\hat{a}_{\alpha\tau i}e^{-ikx} + \hat{b}_{\alpha\tau i}e^{ikx}\right]\right\}.\end{aligned} \tag{A.6}$$

Appendix B

Nonequilibrium free energy

Consider a closed system made of different subsystems, labeled with α. The (average) total entropy production between the final and the initial state obeys the second law of thermodynamics, namely

$$\Delta S_{\rm tot} = \sum_{\alpha} \Delta S_{\alpha} \geq 0. \tag{B.1}$$

We consider one of the subsystems to be a large thermal reservoir, such that its thermal state is not disturbed by the transformation. We refer to this subsystem as the environment (env), which has a well defined temperature $T_{\rm env}$. Applying the first law of thermodynamics to the environment, we obtain

$$T_{\rm env}\Delta S_{\rm env} = \Delta U_{\rm env} - W_{\rm env} \tag{B.2}$$

where $\Delta U_{\rm env}$ is the variation of internal energy of the environment, while $W_{\rm env}$ is the (positive) work performed on the environment reservoir. Using the total energy conservation of the system, namely $\sum_{\alpha} \Delta U_{\alpha} = 0$, we can use the second law in Eq. (B.1) to obtain the thermodynamic maximum of the work performed on the environment. Indeed, we rewrite the second law as

$$T_{\rm env}\Delta S_{\rm tot} = \sum_{\alpha \neq {\rm env}} \left(T_{\rm env}\Delta S_{\alpha} - \Delta U_{\alpha}\right) - W_{\rm env} \geq 0, \tag{B.3}$$

from which we obtain

$$W_{\rm env} \leq -\sum_{\alpha \neq {\rm env}} \Delta F_{\alpha;{\rm env}} = -\sum_{\alpha \neq {\rm env}} \left(\Delta U_{\alpha} - T_{\rm env}\Delta S_{\alpha}\right). \tag{B.4}$$

Here we have defined the thermodynamic quantity $F_{\alpha;{\rm env}} \equiv U_{\alpha} - T_{\rm env}S_{\alpha}$, that we call *nonequilibrium free energy* because of its similarities with the Helmholtz free energy. In particular, since the nonequilibrium free energy only contains the extensive quantities of subsystem α (the internal energy U_{α} and the entropy S_{α}), it does not require the subsystem α to be at local equilibrium. Therefore, as the name suggests, the nonequilibrium free energy accounts also for the possibility of using nonequilibrium resources to produce work.

Bibliography

[1] J. R. Powell, "The Quantum Limit to Moore's Law", Proc. IEEE **96**, 1247–1248 (2008) (cit. on p. 1).

[2] D. P. DiVincenzo, "Quantum Computation", Science **270**, 255–261 (1995) (cit. on p. 1).

[3] F. Giazotto, T. T. Heikkilä, A. Luukanen, A. M. Savin and J. P. Pekola, "Opportunities for mesoscopics in thermometry and refrigeration: Physics and applications", Rev. Mod. Phys. **78**, 217–274 (2006) (cit. on pp. 1, 16).

[4] G. Benenti, G. Casati, K. Saito and R. S. Whitney, "Fundamental aspects of steady-state conversion of heat to work at the nanoscale", Phys. Rep. **694**, 1–124 (2017) (cit. on pp. 1, 16).

[5] I. Žutić, J. Fabian and S. Das Sarma, "Spintronics: Fundamentals and applications", Rev. Mod. Phys. **76**, 323–410 (2004) (cit. on p. 1).

[6] J. P. Pekola, J. M. Kyynäräinen, M. M. Leivo and A. J. Manninen, "NIS chip refrigeration", Cryogenics **39**, 653–657 (1999) (cit. on p. 1).

[7] M. Esposito, K. Lindenberg and C. Van den Broeck, "Thermoelectric efficiency at maximum power in a quantum dot", Europhys. Lett. **85**, 60010 (2009) (cit. on p. 1).

[8] M. Josefsson, A. Svilans, A. M. Burke, E. A. Hoffmann, S. Fahlvik, C. Thelander, M. Leijnse and H. Linke, "A quantum-dot heat engine operating close to the thermodynamic efficiency limits", Nat. Nanotechnol. **13**, 920–924 (2018) (cit. on p. 1).

[9] Y. Rezek, P. Salamon, K. H. Hoffmann and R. Kosloff, "The quantum refrigerator: The quest for absolute zero", Europhys. Lett. **85**, 30008 (2009) (cit. on p. 1).

[10] P. P. Hofer, M. Perarnau-Llobet, J. B. Brask, R. Silva, M. Huber and N. Brunner, "Autonomous quantum refrigerator in a circuit QED architecture based on a Josephson junction", Phys. Rev. B **94**, 235420 (2016) (cit. on p. 1).

[11] A. Vidan, R. M. Westervelt, M. Stopa, M. Hanson and A. C. Gossard, "Triple quantum dot charging rectifier", Appl. Phys. Lett. **85**, 3602–3604 (2004) (cit. on p. 1).

[12]R. Scheibner, M. König, D. Reuter, A. D. Wieck, C. Gould, H. Buhmann and L. W. Molenkamp, "Quantum dot as thermal rectifier", New J. Phys. **10**, 083016 (2008) (cit. on p. 1).

[13]L. Tesser, B. Bhandari, P. A. Erdman, E. Paladino, R. Fazio and F. Taddei, "Heat rectification through single and coupled quantum dots", New J. Phys. **24**, 035001 (2022) (cit. on p. 1).

[14]J. J. Park, K.-H. Kim, T. Sagawa and S. W. Kim, "Heat Engine Driven by Purely Quantum Information", Phys. Rev. Lett. **111**, 230402 (2013) (cit. on p. 2).

[15]J. Yang, C. Elouard, J. Splettstoesser, B. Sothmann, R. Sánchez and A. N. Jordan, "Thermal transistor and thermometer based on Coulomb-coupled conductors", Phys. Rev. B **100**, 045418 (2019) (cit. on p. 2).

[16]M. Acciai, F. Hajiloo, F. Hassler and J. Splettstoesser, "Phase-coherent heat circulators with normal or superconducting contacts", Phys. Rev. B **103**, 085409 (2021) (cit. on p. 2).

[17]S. K. Manikandan, C. Elouard, K. W. Murch, A. Auffèves and A. N. Jordan, "Efficiently fueling a quantum engine with incompatible measurements", Phys. Rev. E **105**, 044137 (2022) (cit. on p. 2).

[18]R. Sánchez, J. Splettstoesser and R. S. Whitney, "Nonequilibrium System as a Demon", Phys. Rev. Lett. **123**, 216801 (2019) (cit. on pp. 2, 46).

[19]F. Hajiloo, R. Sánchez, R. S. Whitney and J. Splettstoesser, "Quantifying nonequilibrium thermodynamic operations in a multiterminal mesoscopic system", Phys. Rev. B **102**, 155405 (2020) (cit. on pp. 2, 46).

[20]R. T. Ross and A. J. Nozik, "Efficiency of hot-carrier solar energy converters", J. Appl. Phys. **53**, 3813–3818 (1982) (cit. on pp. 2, 20).

[21]Ya. M. Blanter and M. Büttiker, "Shot noise in mesoscopic conductors", Phys. Rep. **336**, 1–166 (2000) (cit. on pp. 2, 5, 30, 34).

[22]L. Saminadayar, D. C. Glattli, Y. Jin and B. Etienne, "Observation of the $e/3$ Fractionally Charged Laughlin Quasiparticle", Phys. Rev. Lett. **79**, 2526–2529 (1997) (cit. on pp. 2, 5, 30).

[23]R. De-Picciotto, M. Reznikov, M. Heiblum, V. Umansky, G. Bunin and D. Mahalu, "Direct observation of a fractional charge", Nature **389**, 162–164 (1997) (cit. on pp. 2, 5, 30).

[24]O. S. Lumbroso, L. Simine, A. Nitzan, D. Segal and O. Tal, "Electronic noise due to temperature differences in atomic-scale junctions", Nature **562**, 240–244 (2018) (cit. on pp. 2, 5, 33).

[25]S. Limpert, A. Burke, I.-J. Chen, N. Anttu, S. Lehmann, S. Fahlvik, S. Bremner, G. Conibeer, C. Thelander, M.-E. Pistol and H. Linke, "Single-nanowire, low-bandgap hot carrier solar cells with tunable open-circuit voltage", Nanotechnology **28**, 434001 (2017) (cit. on pp. 2, 21).

[26]I.-J. Chen, S. Limpert, W. Metaferia, C. Thelander, L. Samuelson, F. Capasso, A. M. Burke and H. Linke, "Hot-Carrier Extraction in Nanowire-Nanoantenna Photovoltaic Devices", Nano Lett. **20**, 4064–4072 (2020) (cit. on pp. 2, 21, 22).

[27]J. Fast, E. Barrigon, M. Kumar, Y. Chen, L. Samuelson, M. Borgström, A. Gustafsson, S. Limpert, A. Burke and H. Linke, "Hot-carrier separation in heterostructure nanowires observed by electron-beam induced current", Nanotechnology **31**, 394004 (2020) (cit. on pp. 2, 21).

[28]J. Fast, U. Aeberhard, S. P. Bremner and H. Linke, "Hot-carrier optoelectronic devices based on semiconductor nanowires", Appl. Phys. Rev. **8**, 021309 (2021) (cit. on pp. 2, 21).

[29]J. Fast, Y.-P. Liu, Y. Chen, L. Samuelson, A. M. Burke, H. Linke and A. Mikkelsen, "Optical-Beam-Induced Current in InAs/InP Nanowires for Hot-Carrier Photovoltaics", ACS Appl. Energy Mater. **5**, 7728–7734 (2022) (cit. on pp. 2, 21).

[30]D. Prete, P. A. Erdman, V. Demontis, V. Zannier, D. Ercolani, L. Sorba, F. Beltram, F. Rossella, F. Taddei and S. Roddaro, "Thermoelectric Conversion at 30 K in InAs/InP Nanowire Quantum Dots", Nano Lett. **19**, 3033–3039 (2019) (cit. on pp. 3, 4, 18).

[31]E. T. Jaynes, "Information Theory and Statistical Mechanics", Phys. Rev. **106**, 620–630 (1957) (cit. on p. 3).

[32]H. van Houten, L. W. Molenkamp, C. W. J. Beenakker and C. T. Foxon, "Thermo-electric properties of quantum point contacts", Semicond. Sci. Technol. **7**, B215–B221 (1992) (cit. on pp. 4, 17, 18).

[33]S. F. Svensson, E. A. Hoffmann, N. Nakpathomkun, P. M. Wu, H. Q. Xu, H. A. Nilsson, D. Sánchez, V. Kashcheyevs and H. Linke, "Nonlinear thermovoltage and thermocurrent in quantum dots", New J. Phys. **15**, 105011 (2013) (cit. on pp. 4, 18).

[34]P. Gehring, J. K. Sowa, C. Hsu, J. de Bruijckere, M. van der Star, J. J. Le Roy, L. Bogani, E. M. Gauger and H. S. J. van der Zant, "Complete mapping of the thermoelectric properties of a single molecule", Nat. Nanotechnol. **16**, 426–430 (2021) (cit. on p. 4).

[35]J. B. Johnson, "Thermal Agitation of Electricity in Conductors", Nature **119**, 50–51 (1927) (cit. on p. 4).

[36]H. Nyquist, "Thermal Agitation of Electric Charge in Conductors", Phys. Rev. **32**, 110–113 (1928) (cit. on p. 4).

[37]H. B. Callen and T. A. Welton, "Irreversibility and Generalized Noise", Phys. Rev. **83**, 34–40 (1951) (cit. on p. 4).

[38]M. S. Green, "Markoff Random Processes and the Statistical Mechanics of Time-Dependent Phenomena. II. Irreversible Processes in Fluids", J. Chem. Phys. **22**, 398–413 (1954) (cit. on p. 4).

[39]R. Kubo, "Statistical-Mechanical Theory of Irreversible Processes. I. General Theory and Simple Applications to Magnetic and Conduction Problems", J. Phys. Soc. Jpn. **12**, 570–586 (1957) (cit. on p. 4).

[40]C. Jarzynski, "Nonequilibrium Equality for Free Energy Differences", Phys. Rev. Lett. **78**, 2690–2693 (1997) (cit. on p. 5).

[41]G. E. Crooks, "Nonequilibrium Measurements of Free Energy Differences for Microscopically Reversible Markovian Systems", J. Stat. Phys. **90**, 1481–1487 (1998) (cit. on p. 5).

[42]M. Campisi, P. Hänggi and P. Talkner, "Colloquium: Quantum fluctuation relations: Foundations and applications", Rev. Mod. Phys. **83**, 771–791 (2011) (cit. on p. 5).

[43]C. Van den Broeck and M. Esposito, "Ensemble and trajectory thermodynamics: A brief introduction", Physica A **418**, 6–16 (2015) (cit. on p. 5).

[44]T. R. Gingrich, J. M. Horowitz, N. Perunov and J. L. England, "Dissipation Bounds All Steady-State Current Fluctuations", Phys. Rev. Lett. **116**, 120601 (2016) (cit. on p. 5).

[45]U. Seifert, "Stochastic thermodynamics: From principles to the cost of precision", Physica A **504**, 176–191 (2018) (cit. on p. 5).

[46]S. Kheradsoud, N. Dashti, M. Misiorny, P. P. Potts, J. Splettstoesser and P. Samuelsson, "Power, Efficiency and Fluctuations in a Quantum Point Contact as Steady-State Thermoelectric Heat Engine", Entropy **21**, 777 (2019) (cit. on p. 5).

[47]G. Falasco, M. Esposito and J.-C. Delvenne, "Beyond thermodynamic uncertainty relations: nonlinear response, error-dissipation trade-offs, and speed limits", J. Phys. A: Math. Theor. **55**, 124002 (2022) (cit. on p. 5).

[48]A. A. Kozhevnikov, R. J. Schoelkopf and D. E. Prober, "Observation of Photon-Assisted Noise in a Diffusive Normal Metal–Superconductor Junction", Phys. Rev. Lett. **84**, 3398–3401 (2000) (cit. on p. 5).

[49]X. Jehl, M. Sanquer, R. Calemczuk and D. Mailly, "Detection of doubled shot noise in short normal-metal/ superconductor junctions", Nature **405**, 50–53 (2000) (cit. on p. 5).

[50]Y. Ronen, Y. Cohen, J.-H. Kang, A. Haim, M.-T. Rieder, M. Heiblum, D. Mahalu and H. Shtrikman, "Charge of a quasiparticle in a superconductor", Proc. Natl. Acad. Sci. U.S.A. **113**, 1743–1748 (2016) (cit. on p. 5).

[51]L. Spietz, K. W. Lehnert, I. Siddiqi and R. J. Schoelkopf, "Primary Electronic Thermometry Using the Shot Noise of a Tunnel Junction", Science **300**, 1929–1932 (2003) (cit. on p. 5).

[52]U. Kemiktarak, T. Ndukum, K. C. Schwab and K. L. Ekinci, "Radio-frequency scanning tunnelling microscopy", Nature **450**, 85–88 (2007) (cit. on p. 5).

[53]T. Jullien, P. Roulleau, B. Roche, A. Cavanna, Y. Jin and D. C. Glattli, "Quantum tomography of an electron", Nature **514**, 603–607 (2014) (cit. on p. 5).

[54]R. Bisognin, A. Marguerite, B. Roussel, M. Kumar, C. Cabart, C. Chapdelaine, A. Mohammad-Djafari, J.-M. Berroir, E. Bocquillon, B. Plaçais, A. Cavanna, U. Gennser, Y. Jin, P. Degiovanni and G. Fève, "Quantum tomography of electrical currents", Nat. Commun. **10**, 1–12 (2019) (cit. on p. 5).

[55]E. S. Tikhonov, A. O. Denisov, S. U. Piatrusha, I. N. Khrapach, J. P. Pekola, B. Karimi, R. N. Jabdaraghi and V. S. Khrapai, "Spatial and energy resolution of electronic states by shot noise", Phys. Rev. B **102**, 085417 (2020) (cit. on p. 5).

[56]E. Sivre, H. Duprez, A. Anthore, A. Aassime, F. D. Parmentier, A. Cavanna, A. Ouerghi, U. Gennser and F. Pierre, "Electronic heat flow and thermal shot noise in quantum circuits", Nat. Commun. **10**, 1–8 (2019) (cit. on pp. 5, 33).

[57]S. Larocque, E. Pinsolle, C. Lupien and B. Reulet, "Shot Noise of a Temperature-Biased Tunnel Junction", Phys. Rev. Lett. **125**, 106801 (2020) (cit. on pp. 5, 33, 34).

[58]B. Altaner, M. Polettini and M. Esposito, "Fluctuation-Dissipation Relations Far from Equilibrium", Phys. Rev. Lett. **117**, 180601 (2016) (cit. on pp. 5, 35).

[59]R. Landauer, "Electrical resistance of disordered one-dimensional lattices", Philosophical Magazine: A Journal of Theoretical Experimental and Applied Physics **21**, 863–867 (1970) (cit. on p. 7).

[60]M. Büttiker, Y. Imry, R. Landauer and S. Pinhas, "Generalized many-channel conductance formula with application to small rings", Phys. Rev. B **31**, 6207–6215 (1985) (cit. on p. 7).

[61]M. Büttiker, "Four-Terminal Phase-Coherent Conductance", Phys. Rev. Lett. **57**, 1761–1764 (1986) (cit. on p. 7).

[62]B. J. van Wees, H. van Houten, C. W. J. Beenakker, J. G. Williamson, L. P. Kouwenhoven, D. van der Marel and C. T. Foxon, "Quantized conductance of point contacts in a two-dimensional electron gas", Phys. Rev. Lett. **60**, 848–850 (1988) (cit. on p. 7).

[63]D. A. Wharam, T. J. Thornton, R. Newbury, M. Pepper, H. Ahmed, J. E. F. Frost, D. G. Hasko, D. C. Peacock, D. A. Ritchie and G. A. C. Jones, "One-dimensional transport and the quantisation of the ballistic resistance", J. Phys. C: Solid State Phys. **21**, L209–L214 (1988) (cit. on p. 7).

[64]K. Schwab, E. A. Henriksen, J. M. Worlock and M. L. Roukes, "Measurement of the quantum of thermal conductance", Nature **404**, 974–977 (2000) (cit. on p. 7).

[65]R. de Picciotto, H. L. Stormer, L. N. Pfeiffer, K. W. Baldwin and K. W. West, "Four-terminal resistance of a ballistic quantum wire", Nature **411**, 51–54 (2001) (cit. on p. 7).

[66]M. V. Moskalets, *Scattering Matrix Approach to Non-Stationary Quantum Transport* (World Scientific Publishing Company, London, England, UK, Sept. 2011) (cit. on pp. 7, 41).

[67]G. B. Lesovik and R. Loosen, "On the detection of finite-frequency current fluctuations", Jetp. Lett. **65**, 295–299 (1997) (cit. on p. 12).

[68]D. C. Glattli, "Quantum shot noise of conductors and general noise measurement methods", Eur. Phys. J. Spec. Top. **172**, 163–179 (2009) (cit. on p. 12).

[69]M. Büttiker, "Small normal-metal loop coupled to an electron reservoir", Phys. Rev. B **32**, 1846–1849(R) (1985) (cit. on p. 12).

[70]M. Büttiker, "Role of quantum coherence in series resistors", Phys. Rev. B **33**, 3020–3026 (1986) (cit. on p. 12).

[71]M. J. M. de Jong and C. W. J. Beenakker, "Semiclassical theory of shot noise in mesoscopic conductors", Physica A **230**, 219–248 (1996) (cit. on p. 12).

[72]H. Förster, P. Samuelsson, S. Pilgram and M. Büttiker, "Voltage and dephasing probes in mesoscopic conductors: A study of full-counting statistics", Phys. Rev. B **75**, 035340 (2007) (cit. on p. 12).

[73]K. Brandner, K. Saito and U. Seifert, "Strong Bounds on Onsager Coefficients and Efficiency for Three-Terminal Thermoelectric Transport in a Magnetic Field", Phys. Rev. Lett. **110**, 070603 (2013) (cit. on p. 12).

[74]T. J. Seebeck, "Ueber die magnetische Polarisation der Metalle und Erze durch Temperatur-Differenz", Ann. Phys. **82**, 1–20 (1826) (cit. on p. 15).

[75]J. C. A. Peltier, *Nouvelles expériences sur la caloricité des courans électriques* (1834) (cit. on p. 15).

[76]M. S. Dresselhaus, G. Chen, M. Y. Tang, R. G. Yang, H. Lee, D. Z. Wang, Z. F. Ren, J.-P. Fleurial and P. Gogna, "New Directions for Low-Dimensional Thermoelectric Materials", Adv. Mater. **19**, 1043–1053 (2007) (cit. on p. 15).

[77]R. Kubo, M. Toda and N. Hashitsume, *Statistical Physics II* (Springer, Berlin, Germany) (cit. on p. 16).

[78]H. Pothier, S. Guéron, N. O. Birge, D. Esteve and M. H. Devoret, "Energy Distribution Function of Quasiparticles in Mesoscopic Wires", Phys. Rev. Lett. **79**, 3490–3493 (1997) (cit. on p. 16).

[79]D. S. Golubev, A. D. Zaikin and G. Schön, "On Low-Temperature Dephasing by Electron-Electron Interaction", J. Low Temp. Phys. **126**, 1355–1376 (2002) (cit. on p. 16).

[80]L. W. Molenkamp, Th. Gravier, H. van Houten, O. J. A. Buijk, M. A. A. Mabesoone and C. T. Foxon, "Peltier coefficient and thermal conductance of a quantum point contact", Phys. Rev. Lett. **68**, 3765–3768 (1992) (cit. on p. 16).

[81]S. Jezouin, F. D. Parmentier, A. Anthore, U. Gennser, A. Cavanna, Y. Jin and F. Pierre, "Quantum Limit of Heat Flow Across a Single Electronic Channel", Science **342**, 601–604 (2013) (cit. on p. 16).

[82]S. Gomès, A. Assy and P.-O. Chapuis, "Scanning thermal microscopy: A review", Phys. Status Solidi A **212**, 477–494 (2015) (cit. on p. 16).

[83]S. Roddaro, D. Ercolani, M. A. Safeen, S. Suomalainen, F. Rossella, F. Giazotto, L. Sorba and F. Beltram, "Giant Thermovoltage in Single InAs Nanowire Field-Effect Transistors", Nano Lett. **13**, 3638–3642 (2013) (cit. on pp. 17, 18).

[84]L. D. Hicks and M. S. Dresselhaus, "Effect of quantum-well structures on the thermoelectric figure of merit", Phys. Rev. B **47**, 12727–12731 (1993) (cit. on p. 16).

[85]G. D. Mahan and J. O. Sofo, "The best thermoelectric.", Proc. Natl. Acad. Sci. U.S.A. **93**, 7436–7439 (1996) (cit. on p. 16).

[86]T. E. Humphrey and H. Linke, "Quantum, cyclic, and particle-exchange heat engines", Physica E **29**, 390–398 (2005) (cit. on p. 16).

[87]E. Shapira, A. Holtzman, D. Marchak and Y. Selzer, "Very High Thermopower of Bi Nanowires with Embedded Quantum Point Contacts", Nano Lett. **12**, 808–812 (2012) (cit. on p. 18).

[88]R. S. Whitney, "Most Efficient Quantum Thermoelectric at Finite Power Output", Phys. Rev. Lett. **112**, 130601 (2014) (cit. on pp. 18, 42, 44).

[89]R. S. Whitney, "Finding the quantum thermoelectric with maximal efficiency and minimal entropy production at given power output", Phys. Rev. B **91**, 115425 (2015) (cit. on pp. 18, 42, 44).

[90]A. Svilans, M. Leijnse and H. Linke, "Experiments on the thermoelectric properties of quantum dots", C. R. Phys. **17**, 1096–1108 (2016) (cit. on p. 18).

[91]I.-J. Chen, A. Burke, A. Svilans, H. Linke and C. Thelander, "Thermoelectric Power Factor Limit of a 1D Nanowire", Phys. Rev. Lett. **120**, 177703 (2018) (cit. on p. 18).

[92]L. Onsager, "Reciprocal Relations in Irreversible Processes. II.", Phys. Rev. **38**, 2265–2279 (1931) (cit. on p. 18).

[93]H. B. G. Casimir, "On Onsager's Principle of Microscopic Reversibility", Rev. Mod. Phys. **17**, 343–350 (1945) (cit. on p. 18).

[94]M. Buttiker, "Capacitance, admittance, and rectification properties of small conductors", J. Phys.: Condens. Matter **5**, 9361–9378 (1993) (cit. on p. 18).

[95]N. Dashti, M. Acciai, S. Kheradsoud, M. Misiorny, P. Samuelsson and J. Splettstoesser, "Readout of Quantum Screening Effects Using a Time-Dependent Probe", Phys. Rev. Lett. **127**, 246802 (2021) (cit. on p. 18).

[96]R. S. Whitney, "Nonlinear thermoelectricity in point contacts at pinch off: A catastrophe aids cooling", Phys. Rev. B **88**, 064302 (2013) (cit. on p. 18).

[97]B. K. Ridley, "Hot electrons in low-dimensional structures", Rep. Prog. Phys. **54**, 169–256 (1991) (cit. on p. 20).

[98]W. Shockley and H. J. Queisser, "Detailed Balance Limit of Efficiency of p-n Junction Solar Cells", J. Appl. Phys. **32**, 510–519 (1961) (cit. on p. 20).

[99]A. Othonos, "Probing ultrafast carrier and phonon dynamics in semiconductors", J. Appl. Phys. **83**, 1789–1830 (1998) (cit. on p. 20).

[100]M. A. Green, *Third Generation Photovoltaics* (Springer, Berlin, Germany, 2003) (cit. on p. 20).

[101]P. Würfel, A. S. Brown, T. E. Humphrey and M. A. Green, "Particle conservation in the hot-carrier solar cell", Prog. Photovoltaics Res. Appl. **13**, 277–285 (2005) (cit. on p. 20).

[102]S. Limpert, S. Bremner and H. Linke, "Reversible electron–hole separation in a hot carrier solar cell", New J. Phys. **17**, 095004 (2015) (cit. on p. 20).

[103]S. Kahmann and M. A. Loi, "Hot carrier solar cells and the potential of perovskites for breaking the Shockley–Queisser limit", J. Mater. Chem. C **7**, 2471–2486 (2019) (cit. on p. 21).

[104]G. Manzano, R. Sánchez, R. Silva, G. Haack, J. B. Brask, N. Brunner and P. P. Potts, "Hybrid thermal machines: Generalized thermodynamic resources for multitasking", Phys. Rev. Res. **2**, 043302 (2020) (cit. on p. 27).

[105]F. Battista, F. Haupt and J. Splettstoesser, "Energy and power fluctuations in ac-driven coherent conductors", Phys. Rev. B **90**, 085418 (2014) (cit. on p. 32).

[106]M. Silaev, T. T. Heikkilä and P. Virtanen, "Lindblad-equation approach for the full counting statistics of work and heat in driven quantum systems", Phys. Rev. E **90**, 022103 (2014) (cit. on p. 32).

[107]J. P. Pekola and B. Karimi, "Colloquium: Quantum heat transport in condensed matter systems", Rev. Mod. Phys. **93**, 041001 (2021) (cit. on pp. 32, 33).

[108]J. V. Koski, T. Sagawa, O.-P. Saira, Y. Yoon, A. Kutvonen, P. Solinas, M. Möttönen, T. Ala-Nissila and J. P. Pekola, "Distribution of entropy production in a single-electron box", Nat. Phys. **9**, 644–648 (2013) (cit. on p. 32).

[109]B. Karimi, F. Brange, P. Samuelsson and J. P. Pekola, "Reaching the ultimate energy resolution of a quantum detector", Nat. Commun. **11**, 1–6 (2020) (cit. on p. 32).

[110]J. P. Pekola and B. Karimi, "Ultrasensitive Calorimetric Detection of Single Photons from Qubit Decay", Phys. Rev. X **12**, 011026 (2022) (cit. on p. 32).

[111]S. I. Erlingsson and D. Loss, "Determining the spin Hall conductance via charge transport", Phys. Rev. B **72**, 121310 (2005) (cit. on p. 32).

[112]Y. Tserkovnyak and A. Brataas, "Shot noise in ferromagnet–normal metal systems", Phys. Rev. B **64**, 214402 (2001) (cit. on p. 32).

[113]E. G. Mishchenko, "Shot noise in a diffusive ferromagnetic-paramagnetic-ferromagnetic spin valve", Phys. Rev. B **68**, 100409 (2003) (cit. on p. 32).

[114]J. Meair, P. Stano and P. Jacquod, "Measuring spin accumulations with current noise", Phys. Rev. B **84**, 073302 (2011) (cit. on p. 32).

[115]T. Arakawa, J. Shiogai, M. Ciorga, M. Utz, D. Schuh, M. Kohda, J. Nitta, D. Bougeard, D. Weiss, T. Ono and K. Kobayashi, "Shot Noise Induced by Nonequilibrium Spin Accumulation", Phys. Rev. Lett. **114**, 016601 (2015) (cit. on pp. 32, 39).

[116] A. Rosenblatt, S. Konyzheva, F. Lafont, N. Schiller, J. Park, K. Snizhko, M. Heiblum, Y. Oreg and V. Umansky, "Energy Relaxation in Edge Modes in the Quantum Hall Effect", Phys. Rev. Lett. **125**, 256803 (2020) (cit. on p. 33).

[117] R. A. Melcer, B. Dutta, C. Spånslätt, J. Park, A. D. Mirlin and V. Umansky, "Absent thermal equilibration on fractional quantum Hall edges over macroscopic scale", Nat. Commun. **13**, 1–7 (2022) (cit. on p. 33).

[118] E. Zhitlukhina, M. Belogolovskii and P. Seidel, "Electronic noise generated by a temperature gradient across a hybrid normal metal–superconductor nanojunction", Appl. Nanosci. **10**, 5121–5124 (2020) (cit. on p. 33).

[119] J. Rech, T. Jonckheere, B. Grémaud and T. Martin, "Negative Delta-T Noise in the Fractional Quantum Hall Effect", Phys. Rev. Lett. **125**, 086801 (2020) (cit. on p. 33).

[120] M. Hasegawa and K. Saito, "Delta-T noise in the Kondo regime", Phys. Rev. B **103**, 045409 (2021) (cit. on p. 33).

[121] A. Popoff, J. Rech, T. Jonckheere, L. Raymond, B. Grémaud, S. Malherbe and T. Martin, "Scattering theory of non-equilibrium noise and delta T current fluctuations through a quantum dot", J. Phys.: Condens. Matter **34**, 185301 (2022) (cit. on p. 33).

[122] G. Zhang, I. V. Gornyi and C. Spånslätt, "Delta-T noise for weak tunneling in one-dimensional systems: Interactions versus quantum statistics", Phys. Rev. B **105**, 195423 (2022) (cit. on p. 33).

[123] D. Gresta, M. Real and L. Arrachea, "Optimal Thermoelectricity with Quantum Spin Hall Edge States", Phys. Rev. Lett. **123**, 186801 (2019) (cit. on p. 38).

[124] C. Wu, B. A. Bernevig and S.-C. Zhang, "Helical Liquid and the Edge of Quantum Spin Hall Systems", Phys. Rev. Lett. **96**, 106401 (2006) (cit. on p. 38).